AIAA JOURNAL
Vol. 47, No. 3, March 2009

# Dynamics Modeling and Simulation of Flexible Airships

Yuwen Li,* Meyer Nahon,† and Inna Sharf‡
*McGill University, Montreal, Quebec H3A 2K6, Canada*

DOI: 10.2514/1.37455

**A new dynamics modeling approach is proposed for flexible airships, which integrates the flight dynamics, structural dynamics, aerostatics, and aerodynamics. In particular, a comprehensive aerodynamic computation is presented, including the potential-flow aerodynamics, the viscous effects, the forces on the fins, the forces on the hull due to the fins, and the axial drag. The coupling between flexibility and aerodynamics is incorporated through the local velocity of the deformed airship. The resulting dynamics model is represented by a single set of nonlinear ordinary differential equations, describing the rigid-body motion, the elastic deformation, and the coupling between them. This model has been implemented and used to simulate the Skyship-500 airship. Simulation results demonstrate the effects of structural flexibility on the aerodynamic and dynamic characteristics of the vehicle. These results reveal that strong coupling exists between the roll rotation and the bending deflection in the lateral plane, and that the natural frequencies of the airship in air are much lower than those in vacuum. In addition, the nonlinear dynamics model is numerically linearized to investigate the aeroelastic stability of the airship.**

## Nomenclature

| | | |
|---|---|---|
| $\mathbf{A}$, $\mathbf{B}$ | = | state matrix and input matrix of the linear model, respectively |
| $b$ | = | fin semispan |
| $C_{\mathrm{DC}}$ | = | crossflow drag coefficient on the hull |
| $C_{L\alpha}$, $C_{l\alpha}$ | = | 3-D and 2-D lift curve slopes of the fins |
| $d_F$ | = | distance from a point on a fin to a point on the hull centerline |
| $E$, $EI$ | = | elastic modulus and bending stiffness |
| $\mathbf{F}$ | = | force vector |
| $\mathbf{f}$ | = | force per unit length along the centerline |
| $g$, $\hat{\mathbf{g}}$ | = | acceleration of gravity and unit direction vector of gravity |
| $\mathbf{I}$ | = | shape function integral |
| $\mathbf{K}$ | = | elastic stiffness matrix of the flexible airship |
| $L$ | = | length of the airship |
| $\mathbf{M}$ | = | moment vector |
| $m$ | = | total mass of the airship |
| $\mathbf{M}_{\mathrm{sys}}$, $\mathbf{M}_{\mathrm{AT}}$ | = | total mass and added-mass matrices |
| $\mathbf{n}$ | = | unit normal vector of the body surface |
| $\mathbf{Q}$ | = | generalized elastic force vector |
| $\mathbf{q}$ | = | generalized elastic coordinate vector |
| $q_0$ | = | dynamic pressure |
| $R$ | = | hull cross-sectional radius |
| $\mathbf{r}$ | = | position vector of a material point from the body-frame origin on the undeformed airship |
| $S$ | = | hull cross-sectional area |
| $\mathcal{T}_f$ | = | kinetic energy of the potential fluid |
| $\overline{\mathbf{U}}$, $\Delta\mathbf{U}$ | = | equilibrium control input and disturbance in control input |
| $\mathbf{u}$ | = | elastic displacement |
| $u_{V,d}$, $v_{V,d}$, $w_{V,d}$ | = | local velocity components at the position $\varepsilon_V$ on the deformed airship expressed in the local centerline frame |
| $V_B$ | = | airship volume |
| $\mathbf{v}$ | = | velocity distribution over the flexible airship |
| $\mathbf{v}_0 = [u_0, v_0, w_0]^T$ | = | linear velocity |
| $\mathbf{v}_d$ | = | local velocity on the deformed airship expressed in the local centerline frame |
| $\overline{\mathbf{X}}$, $\Delta\mathbf{X}$ | = | equilibrium state vector and disturbance in state vector |
| $x$, $y$, $z$ | = | coordinates of a point in the body frame |
| $\alpha_F$ | = | fin angle of attack |
| $\gamma$ | = | angle between centerline and velocity vector |
| $\Delta C_{p\alpha}$ | = | $\partial \Delta C_p / \partial \alpha$, where $\Delta C_p$ is the pressure coefficient of the airfoil |
| $\varepsilon$ | = | longitudinal distance from the nose |
| $\eta$ | = | efficiency factor for the crossflow drag due to finite length |
| $\rho$ | = | air density |
| $\sigma$, $\omega_d$ | = | real and imaginary parts of eigenvalue of the state matrix |
| $\Phi$ | = | total velocity potential |
| $\mathbf{\Psi}_i$ | = | the $i$th shape function |
| $\boldsymbol{\omega} = [p, q, r]^T$ | = | angular velocity |

*Subscripts*

| | | |
|---|---|---|
| AD | = | aerodynamics |
| AS | = | aerostatics |
| axial | = | axial drag |
| $C$ | = | control |
| $F$ | = | aerodynamic force acting on the fins |
| $G$ | = | gravity |
| $H(F)$ | = | aerodynamic force acting on the hull due to the fins |
| $I$ | = | inertial |
| $P$ | = | potential-flow aerodynamics |
| $T$ | = | thrust |
| $V$ | = | viscous aerodynamic effect on the hull |
| $\delta$ | = | aerodynamic force due to control surface deflection |

## I. Introduction

THE resurgence of airships in the past few years has created a need for accurate dynamics models and simulation tools to

Presented as Paper 2212 at the 48th AIAA/ASME/ASCE/AHS/ASC Structures, Structural Dynamics, and Materials Conference, Honolulu, HI, 23–26 April 2007; received 10 March 2008; revision received 27 November 2008; accepted for publication 28 November 2008. 

*Ph.D. Candidate, Department of Mechanical Engineering, 817 Sherbrooke Street West; liyuwen@cim.mcgill.ca.

†Associate Professor, Department of Mechanical Engineering, 817 Sherbrooke Street West; Meyer.Nahon@mcgill.ca. Associate Fellow AIAA.

‡Associate Professor, Department of Mechanical Engineering, 817 Sherbrooke Street West; Inna.Sharf@mcgill.ca. Member AIAA.

study their flight behavior and design their control systems [1]. Several airship dynamics models have been presented in literature. Tischler et al. [2] derived the nonlinear equations of motion and developed the simulation program HLASIM for the design of heavy lift airships. Jex and Gelhausen [3] and Amann [4] applied different aerodynamic computational methods to predict the control responses of the Skyship-500 airship. Analytical linear dynamics models using aerodynamic derivatives were also applied to study the flight stability and control design of airships [5,6]. Li and Nahon [7] proposed a modeling procedure for airship dynamics simulation and validated their model with published experimental data. In all these works, the airship was modeled as a rigid-body vehicle with 6 degrees of freedom (DOF). However, real airships experience deformations and their structural flexibility has been an important consideration in the history of airship development. For example, Evans and DeLaurier [8] computed the force distribution for the Shenandoah rigid airship and demonstrated the possibilities of static structural failure due to the resulting bending moment.

To avoid the structural vulnerability, rigid airships are seldom used nowadays and most modern airships are nonrigid airships (blimps). The static deflection behavior of nonrigid airships was investigated by using a bending beam model [1] and experiments showed that such a model provided reasonable accuracy [9]. With more recent advances in computational capabilities, finite element analysis (FEA) and computational fluid dynamics packages have been used for the preliminary analysis of the static deformations and aerodynamic derivatives of flexible airships and other lighter-than-air (LTA) vehicles [10–13]. However, the effects of structural flexibility on the airships' flight dynamics were not discussed in these works. Bennaceur et al. [14] investigated the equations of motion of a flexible airship with a particular focus on the effects of deformation on the inertial force. Nevertheless, their formulation was limited by assuming the air to be a potential fluid, and little discussion was given on the interaction between the flexibility and the aerodynamic forces.

Although few prior papers exist on the influence of deformation on the aerodynamics and flight dynamics of LTA aircraft, there has been an increasing interest in the modeling of the interaction of flexibility, aerodynamics, and flight dynamics of a maneuvering heavier-than-air (HTA) aircraft, especially because powerful computers are available to solve such complicated problems. For example, Schmidt [15] and Meirovitch and Tuzcu [16] presented different modeling methods to unify the analysis of flight dynamics, structural dynamics, aerodynamics, and control system for flexible airplanes. Platus [17] derived the equations of motion for a spinning missile and demonstrated that the interaction between the bending, aerodynamic force and roll rotation could cause aeroelastic instability. Patil and Hodges [18] and Cesnik and Su [19] investigated the effects of deformation on the flight stability and the time response of the rigid-body motion for a pair of highly flexible flying wings and a fully flexible joined-wing vehicle, respectively. A more detailed literature review of the theoretical dynamics models of flexible HTA aircraft can be found in [16].

Generally speaking, existing airship dynamics models focus on the interaction of inertial and aerodynamic forces, whereas the effects of structural flexibility are seldom discussed. The dynamics modeling techniques of flexible airships have lagged behind those for HTA aircraft, and the motivation for this research is to fill this gap. For this purpose, a general dynamics modeling approach is proposed for flexible airships, which integrates the flight dynamics, structural dynamics, aerostatics, and aerodynamics. The primary motivation of the present work was to present a modeling framework to analyze a wide range of airship designs, including conventional ones or those now being proposed for stratospheric or planetary exploration applications. In the present work, our theoretical model is implemented in software and used to calculate the time and frequency responses to elevator and rudder inputs for a particular conventional airship: the Skyship-500, for which inertial and geometric data are available in the open literature. Finally, the nonlinear equations of motion are linearized to analyze the aeroelastic stability of the vehicle, and a simplified model is also shown toward this same purpose. To the authors' knowledge, this is the first theoretical work on the aeroelastic stability of LTA vehicles.

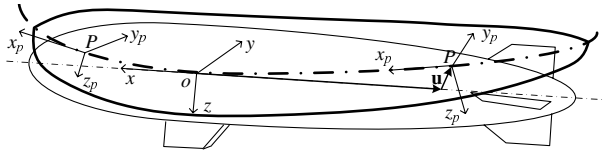


**Fig. 1 Body frame on the undeformed body and centerline frames.**

## II. Equations of Motion

### A. Kinematic Description

Following the lead in [16], we write the equations of motion of a flexible airship in a body frame $\{oxyz\}$ fixed on the undeformed airship (as shown in Fig. 1), with its origin $o$ at the center of volume (c.v.), the $x$ axis along the hull centerline and pointing toward the nose, the $z$ axis vertically downward, and the positive $y$ axis determined by the right-hand rule. The motion of the vehicle is then described as the translation and rotation of this body frame with respect to an inertial frame fixed on the ground, plus the deformation of the material points on the body relative to the body frame. In addition, a *local* centerline frame $\{Px_py_pz_p\}$ will be used in the aerodynamics computation for a flexible airship in Sec. III. This frame is established along the centerline of the deformed airship at a point $P$, with its $x_p$ axis tangent to the centerline, and its orientation is related to the local deformation.

With the aforementioned body-fixed frame assignment, the elastic displacement $\mathbf{u}$ of a material point on the airship is written as a summation of shape functions according to[§]

$$\mathbf{u} = \sum q_i(t)\boldsymbol{\Psi}_i(\mathbf{r}) \tag{1}$$

where $q_i$ are the time-dependent generalized elastic coordinates, $\boldsymbol{\Psi}_i = [\Psi_{xi}, \Psi_{yi}, \Psi_{zi}]^T$ are the time-independent shape functions, and $\mathbf{r}$ is the position vector of the material point from the origin $o$ on the undeformed body expressed in the body-fixed frame. Then, the velocity distribution over the elastic body is expressed as

$$\mathbf{v} = \mathbf{v}_0 + \boldsymbol{\omega}^{\times}\mathbf{r} + \boldsymbol{\omega}^{\times}\mathbf{u} + \dot{\mathbf{u}} \tag{2}$$

where $\mathbf{v}_0 = [u_0, v_0, w_0]^T$, $\boldsymbol{\omega} = [p, q, r]^T$ denote the linear and angular velocity vectors, respectively. The superscript $\times$ denotes the skew-symmetric matrix form of a vector (corresponding to a crossproduct operation). The first two terms in Eq. (2) are associated with the rigid-body translation and rotation, respectively, and the last two terms represent the influence of the flexibility on the local velocity. It is noted that $\mathbf{v}_0$ is not the total contribution to the velocity of the *material* point at the c.v., which must include the deformation terms in Eq. (2).

In this work, the shape functions employed in Eq. (1) are chosen as the natural vibration mode shapes of a free–free Euler–Bernoulli beam undergoing bending deformation only. There are three principal reasons for using this simplified model to describe flexibility of the airship. First, from published FEA results of modal analysis of an airship with a fineness ratio of 4 [11] and an ellipsoidal shell with a fineness ratio of 6 [13], the fundamental mode shape of an airship usually describes the hull bending if the internal pressure is high enough to prevent wrinkling. Second, the deflection characteristics of nonrigid airships have been investigated using an Euler–Bernoulli beam model [1], and experiments on airship models

[§]As much as possible, the authors tried to follow conventional notations used in the different fields pertaining to this paper. This, however, resulted in a number of notational conflicts: the same symbol used to denote different physical variables. Where deemed not detrimental to the presentation, some of the original conventions were changed, but several conflicts still remain. For example, $q$ usually denotes a generalized coordinate in the context of structural analysis, a pitch rate in flight dynamics, and dynamic pressure in aerodynamics.

(with fineness ratios of 4, 6.9, and 8.5) have shown that such a model provided reasonable accuracy [9]. Third, experimental and theoretical studies have shown that Euler–Bernoulli beam models can be successfully employed to analyze the deflection behavior of inflated cylinders with fineness ratios from 6 to 18 without wrinkling [20,21]. A Timoshenko beam model or a finite-element-based method [22] can be applied to incorporate more comprehensive deformation models, but would require more complicated modeling.

We employ $2N$ shape functions to describe the airship's deflection. The first $N$ shape functions are chosen as $\boldsymbol{\Psi}_i = [0, \Psi_i, 0]^T$, $i = 1, 2, \ldots, N$, describing the bending in the $oxy$ plane, and the other $N$ shape functions are written as $\boldsymbol{\Psi}_{N+i} = [0, 0, \Psi_i]^T$, $i = 1, 2, \ldots, N$, describing the bending in the $oxz$ plane, where $\Psi_i$ is the $i$th natural mode shape of the free–free Euler–Bernoulli beam.

### B. Equations of Motion

Given the velocity distribution in Eq. (2) and the shape functions introduced in Sec. II.A, the dynamics equations of an elastic vehicle can be derived by a number of procedures [16] and can be summarized in the following matrix form:

$$\begin{bmatrix} \mathbf{M}_{11} & \mathbf{M}_{12} & \mathbf{M}_{13} \\ \mathbf{M}_{21} & \mathbf{M}_{22} & \mathbf{M}_{23} \\ \mathbf{M}_{31} & \mathbf{M}_{32} & \mathbf{M}_{33} \end{bmatrix} \begin{bmatrix} \dot{\mathbf{v}}_0 \\ \dot{\boldsymbol{\omega}} \\ \ddot{\mathbf{q}} \end{bmatrix} = -\begin{bmatrix} \mathbf{0} \\ \mathbf{0} \\ \mathbf{K}\mathbf{q} \end{bmatrix} + \begin{bmatrix} \mathbf{F}_I \\ \mathbf{M}_I \\ \mathbf{Q}_I \end{bmatrix} + \begin{bmatrix} \mathbf{F}_G \\ \mathbf{M}_G \\ \mathbf{Q}_G \end{bmatrix} + \begin{bmatrix} \mathbf{F}_{\mathrm{AS}} \\ \mathbf{M}_{\mathrm{AS}} \\ \mathbf{Q}_{\mathrm{AS}} \end{bmatrix} + \begin{bmatrix} \mathbf{F}_{\mathrm{AD}} \\ \mathbf{M}_{\mathrm{AD}} \\ \mathbf{Q}_{\mathrm{AD}} \end{bmatrix} + \begin{bmatrix} \mathbf{F}_C \\ \mathbf{M}_C \\ \mathbf{Q}_C \end{bmatrix} \tag{3}$$

where $\mathbf{q} = [q_1, q_2, \ldots, q_{2N}]^T$ is the generalized elastic coordinate vector, the coefficient matrix on the left-hand side, later abbreviated to $\mathbf{M}_{\mathrm{sys}}$, is the $(6 + 2N) \times (6 + 2N)$ symmetric mass matrix of the flexible airship, and, in particular, $\mathbf{M}_{33}$ is the elastic generalized mass matrix. The nonzero elements of the stiffness matrix $\mathbf{K}$ can be computed as

$$K_{i,j} = K_{N+i,N+j} = \int_L EI\Psi_i''\Psi_j'' \,\mathrm{d}x, \qquad i, j = 1, 2, \ldots, N \tag{4}$$

where $EI$ is the bending stiffness and $\Psi_i'' = d^2\Psi_i/dx^2$. The subscripts $I$, $G$, AS, AD, and $C$ on the right-hand side of Eq. (3) denote the forces and moments due to inertia, gravity, aerostatics, aerodynamics, and control, respectively. The expressions for the mass matrix $\mathbf{M}_{\mathrm{sys}}$ and the inertial terms $\mathbf{F}_I$, $\mathbf{M}_I$, and $\mathbf{Q}_I$ of an elastic body have been derived previously in the context of flexible HTA aircraft [22] and robotic manipulators [23] and are the same for an elastic airship. The gravitational, aerostatic, and thrust forces are defined in the following subsection, and the aerodynamic terms are discussed in Sec. III.

### C. Gravity, Aerostatic, and Thrust Forces

The airship flexibility does not affect the magnitude of the gravitational force, that is, $\mathbf{F}_G = mg\hat{\mathbf{g}}$, where $m$ is the total mass of the vehicle, including the hull, gas, gondola, fins, ballonets, etc.; $g$ is the acceleration of gravity; and $\hat{\mathbf{g}}$ is the unit vector in the direction of gravity. However, the gravitational moment is affected by the deformation because of the elastic displacement of the center of gravity (c.g.), which is computed as

$$\mathbf{u}_G = \int_m \mathbf{u} \,\mathrm{d}m/m$$

Substituting Eq. (1) for $\mathbf{u}$ leads to

$$\mathbf{u}_G = \frac{1}{m}\sum_{i=1}^{2N} q_i(t)\mathbf{p}_i$$

where

$$\mathbf{p}_i = \int_m \boldsymbol{\Psi}_i \,\mathrm{d}m$$

is the $i$th linear momentum coefficient [22], and the external moment due to gravity is then computed as

$$\mathbf{M}_G = \mathbf{r}_G^{\times}\mathbf{F}_G + \frac{1}{m}\sum_{i=1}^{2N} q_i(t)\mathbf{p}_i^{\times}\mathbf{F}_G \tag{5}$$

Components of the gravitational generalized force are computed as

$$Q_{Gi} = \int_m g\hat{\mathbf{g}}^T\boldsymbol{\Psi}_i \,\mathrm{d}m = g\hat{\mathbf{g}}^T\mathbf{p}_i, \qquad i = 1, 2, \ldots, 2N \tag{6}$$

The aerostatic force can be computed as $\mathbf{F}_{\mathrm{AS}} = -\rho g V_B \hat{\mathbf{g}}$, assuming that the flexibility does not affect the body volume $V_B$. For a rigid-body airship, the aerostatic moment is zero because the body frame is located at the c.v.; whereas, for a flexible airship, the elastic displacement of c.v. must be incorporated, which is computed as

$$\mathbf{u}_V = \frac{1}{V_B}\int_{V_B} \mathbf{u} \,\mathrm{d}V$$

Then, substituting Eq. (1) to determine $\mathbf{u}_V$, the external moment due to aerostatics can be written as

$$\mathbf{M}_{\mathrm{AS}} = \sum_{i=1}^{2N} q_i \mathbf{I}_{\mathrm{AS},i}^{\times}\mathbf{F}_{\mathrm{AS}}$$

where we define the aerostatic shape function integral $\mathbf{I}_{\mathrm{AS},i}$ for the $i$th mode as

$$\mathbf{I}_{\mathrm{AS},i} = \frac{1}{V_B}\int_{V_B} \boldsymbol{\Psi}_i \,\mathrm{d}V = \frac{1}{V_B}\int_L \boldsymbol{\Psi}_i S \,\mathrm{d}x \tag{7}$$

where $S$ is the cross-sectional area of the hull. The aerostatic generalized force is computed as

$$Q_{\mathrm{AS},i} = -\int_L \rho g \hat{\mathbf{g}}^T\boldsymbol{\Psi}_i S \,\mathrm{d}x$$

or, using the shape function of Eq. (7), we have

$$Q_{\mathrm{AS},i} = \mathbf{F}_{\mathrm{AS}}^T\mathbf{I}_{\mathrm{AS},i}, \qquad i = 1, 2, \ldots, 2N \tag{8}$$

Unlike the distributed gravitational and aerostatic forces, the thrust forces are modeled as concentrated forces. The moment due to a thrust force is then calculated as

$$\mathbf{M}_T = \mathbf{r}_T^{\times}\mathbf{F}_T + \sum_{i=1}^{2N} q_i(t)\boldsymbol{\Psi}_i(\mathbf{r}_T)^{\times}\mathbf{F}_T \tag{9}$$

where $\mathbf{F}_T = [F_T, 0, 0]^T$, $F_T$ is the thrust force, $\mathbf{r}_T$ denotes the position at which the thruster is mounted, and $\boldsymbol{\Psi}_i(\mathbf{r}_T)$ is the shape function evaluated at this position. The corresponding generalized force is then given by $Q_{Ti} = \mathbf{F}_T^T\boldsymbol{\Psi}_i(\mathbf{r}_T)$. We can see that the influence of flexibility on the thruster model is incorporated in the moment calculation by accounting for the elastic displacement at the thruster position.

## III. Aerodynamics

To complete the dynamics model, the aerodynamic force, moment, and generalized force must be incorporated into Eq. (3). This is accomplished here by extending the computational approach for a rigid aircraft developed previously in [7]. In this approach, the aerodynamic forces are categorized into various terms based on different physical effects, and the aerodynamic formulation can be summarized as follows:

$$\begin{bmatrix}\mathbf{F}_{\text{AD}}\\ \mathbf{M}_{\text{AD}}\\ \mathbf{Q}_{\text{AD}}\end{bmatrix}=\begin{bmatrix}\mathbf{F}_P\\ \mathbf{M}_P\\ \mathbf{Q}_P\end{bmatrix}+\begin{bmatrix}\mathbf{F}_V\\ \mathbf{M}_V\\ \mathbf{Q}_V\end{bmatrix}+\begin{bmatrix}\mathbf{F}_F\\ \mathbf{M}_F\\ \mathbf{Q}_F\end{bmatrix}+\begin{bmatrix}\mathbf{F}_{H(F)}\\ \mathbf{M}_{H(F)}\\ \mathbf{Q}_{H(F)}\end{bmatrix}+\begin{bmatrix}\mathbf{F}_{\text{axial}}\\ \mathbf{M}_{\text{axial}}\\ \mathbf{Q}_{\text{axial}}\end{bmatrix} \tag{10}$$

where the first term represents the potential-flow aerodynamics related to the added mass, the second term is due to the viscous effect on the hull, the third term is the force acting on the fins, the fourth term is the force on the hull due to the fins, and the last term is associated with the axial drag. The computation of each term will be discussed in the following subsections but first we revisit the velocity distribution of a flexible airship employed in these computations.

To consider the effects of flexibility on the aerodynamics, the local velocity components defined in the local centerline frame $\{Px_py_pz_p\}$ (shown in Fig. 1) are used in the aerodynamics computation for a flexible airship. For small elastic displacements and infinitesimal rotations, we use the first-order approximation to compute the rotation matrix from the body frame to the local centerline frame [23], and the velocity distribution of a flexible airship, that is, $\mathbf{v}$ from Eq. (2), is then rewritten in the local centerline frame $\{Px_py_pz_p\}$. Neglecting the products of the following terms of small orders of magnitude, $(p, q, r, \Psi_i, \Psi_i')$, we have

$$\mathbf{v}_d \approx \mathbf{v}_0 + \boldsymbol{\omega}^{\times}\mathbf{r} + \sum_{i=1}^{2N}\dot{q}_i\boldsymbol{\Psi}_i - u_0\sum_{i=1}^{2N}q_i\boldsymbol{\Psi}_i' \tag{11}$$

where the subscript $d$ denotes a vector written in a local centerline frame on the deformed body, and $\boldsymbol{\Psi}_i' = \mathrm{d}\boldsymbol{\Psi}_i/\mathrm{d}x$. The last two terms in Eq. (11) represent the influence of deformation: one related to the deflection rate and the other related to the bending slope. To incorporate the effects of flexibility, $\mathbf{v}_d$ from Eq. (11) is used in the aerodynamics computations.

### A. Potential-Flow Aerodynamic Force

For a rigid-body vehicle completely submerged in an unbounded potential fluid, the fluid kinetic energy can be written in terms of a $6 \times 6$ added-mass matrix, and the aerodynamic force can be written in terms of the added-mass matrix [24]. For a flexible vehicle, with its deformation described by $2N$ shape functions, the added-mass matrix representing the fluid kinetic energy should be a $(6 + 2N) \times (6 + 2N)$ matrix. To the authors' knowledge, no works have been published on a complete formulation of the added-mass matrix and the potential-flow aerodynamic forces and moments for an elastic vehicle maneuvering in a heavy fluid. In this subsection, the derivation of this added-mass matrix and the computation of the corresponding aerodynamic forces and moments are presented from first principles. For this purpose, the boundary condition of the Laplace equation is first given for an elastic vehicle, then the corresponding aerodynamic forces, moments, and generalized forces are derived from the fluid's kinetic energy.

#### 1. *Boundary Condition of the Laplace Equation*

For a potential fluid, the velocity vector of the fluid $\mathbf{v}_f$ can be represented by the gradient of a scalar potential $\Phi$ [24], that is, $\mathbf{v}_f = \nabla\Phi$, and the continuity equation for the fluid is $\nabla^2\Phi = 0$ [24]. In the case of a vehicle in an unbounded fluid, no fluid particles can flow through the boundary surface into the body, and so at a point on the surface boundary, the normal component of the fluid velocity must be equal to the normal velocity of that point on the body, as shown in Fig. 2, that is, $\mathbf{v}_f^T\mathbf{n} = \mathbf{v}_d^T\mathbf{n}$, where $\mathbf{n}$ is the unit normal vector of the boundary surface $S_B$, with its positive direction defined pointing outward from the body. Substituting $\mathbf{v}_d$ from Eq. (11) into $\mathbf{v}_f^T\mathbf{n} = \mathbf{v}_d^T\mathbf{n}$, we obtain the boundary conditions of the Laplace equation for a flexible body moving through an unbounded potential fluid:

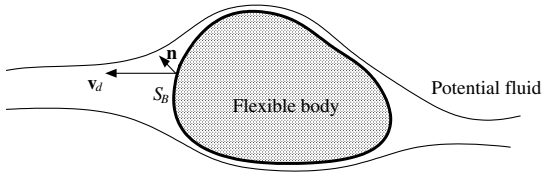


**Fig. 2 Boundary condition of the Laplace equation.**

$$\mathbf{v}_f^T\mathbf{n} = \mathbf{v}_0^T\mathbf{n} + \boldsymbol{\omega}^T(\mathbf{r}^{\times}\mathbf{n}) + \sum_{i=1}^{2N}\dot{q}_i\boldsymbol{\Psi}_i^T\mathbf{n} - u_0\sum_{i=1}^{2N}q_i\boldsymbol{\Psi}_i'^T\mathbf{n}, \quad \text{over} \quad S_B \tag{12}$$

To separate the variables according to the boundary conditions, we write the velocity potential as a superposition of various velocity potential components:

$$\Phi = \boldsymbol{\upsilon}^T\boldsymbol{\Phi}_r + \dot{\mathbf{q}}^T\boldsymbol{\Phi}_q + u_0\mathbf{q}^T\boldsymbol{\Phi}_s \tag{13}$$

where $\boldsymbol{\upsilon} = [\mathbf{v}_0^T, \boldsymbol{\omega}^T]^T$. The vector $\boldsymbol{\Phi}_r = [\Phi_{r1}, \Phi_{r2}, \ldots, \Phi_{r6}]^T$ represents the velocity potentials associated with the rigid-body motion, in which $\boldsymbol{\Phi}_{r1} = [\Phi_{r1}, \Phi_{r2}, \Phi_{r3}]^T$ contains the potential components related to the translational motion and $\boldsymbol{\Phi}_{r2} = [\Phi_{r4}, \Phi_{r5}, \Phi_{r6}]^T$ contains those related to the rotational motion. The vector $\boldsymbol{\Phi}_q = [\Phi_{q1}, \Phi_{q2}, \ldots, \Phi_{q2N}]^T$ denotes the potential components related to the mode shapes, and the vector $\boldsymbol{\Phi}_s = [\Phi_{s1}, \Phi_{s2}, \ldots, \Phi_{s2N}]^T$ includes the components associated with the slopes of the shape functions. The potentials $\Phi_{ri}, \Phi_{qi}, \Phi_{si}$ are functions of position only; they satisfy the Laplace equation and the following boundary conditions: $\partial\boldsymbol{\Phi}_{r1}/\partial n = \mathbf{n}$, $\partial\boldsymbol{\Phi}_{r2}/\partial n = \mathbf{r}^{\times}\mathbf{n}$, $\partial\Phi_{qi}/\partial n = \boldsymbol{\Psi}_i^T\mathbf{n}$, and $\partial\Phi_{si}/\partial n = -\boldsymbol{\Psi}_i'^T\mathbf{n}$, with components $\partial\Phi_{r1}/\partial n \equiv (\nabla\Phi_{r1})^T\mathbf{n}$, etc. Under these boundary conditions, we can check that the velocity potential in Eq. (13) is a solution of the Laplace equation with the boundary conditions of a flexible vehicle in Eq. (12).

#### 2. *Fluid Kinetic Energy*

With the velocity of the fluid represented by the velocity potential, the kinetic energy of the fluid is

$$\mathcal{T}_f = \frac{1}{2}\rho\iiint_{V_f}(\nabla\Phi)^T(\nabla\Phi)\,\mathrm{d}V$$

in which $V_f$ denotes the fluid volume, and, using Green's theorem, we have

$$\mathcal{T}_f = -\frac{1}{2}\rho\iint_{S_B}\Phi\frac{\partial\Phi}{\partial n}\,\mathrm{d}S$$

With the velocity potential written as the superposition of $\Phi_{ri}$, $\Phi_{qi}$, and $\Phi_{si}$ from Eq. (13), we have

$$\begin{aligned}\mathcal{T}_f = {}& \tfrac{1}{2}\boldsymbol{\upsilon}^T\mathbf{M}_{rr}\boldsymbol{\upsilon} + \tfrac{1}{2}\dot{\mathbf{q}}^T\mathbf{M}_{qq}\dot{\mathbf{q}} + \tfrac{1}{2}u_0^2\mathbf{q}^T\mathbf{M}_{ss}\mathbf{q} + \tfrac{1}{2}u_0\mathbf{q}^T\mathbf{M}_{sq}\dot{\mathbf{q}}\\ & + \tfrac{1}{2}u_0\dot{\mathbf{q}}^T\mathbf{M}_{qs}\mathbf{q} + \tfrac{1}{2}\boldsymbol{\upsilon}^T\mathbf{M}_{rq}\dot{\mathbf{q}} + \tfrac{1}{2}\dot{\mathbf{q}}^T\mathbf{M}_{qr}\boldsymbol{\upsilon} + \tfrac{1}{2}u_0\mathbf{q}^T\mathbf{M}_{sr}\boldsymbol{\upsilon}\\ & + \tfrac{1}{2}u_0\boldsymbol{\upsilon}^T\mathbf{M}_{rs}\mathbf{q}\end{aligned} \tag{14}$$

where the time-independent added-mass matrices $\mathbf{M}_{rr}$, $\mathbf{M}_{rq}$, $\mathbf{M}_{qr}$, $\mathbf{M}_{qq}$, $\mathbf{M}_{rs}$, $\mathbf{M}_{sr}$, $\mathbf{M}_{sq}$, $\mathbf{M}_{qs}$, and $\mathbf{M}_{ss}$ are constructed from the $i$, $j$ entries defined in Table 1. The matrix $\mathbf{M}_{rr}$ is a $6 \times 6$ rigid-body added-mass matrix; $\mathbf{M}_{rq}$, $\mathbf{M}_{qr}$ and $\mathbf{M}_{rs}$, $\mathbf{M}_{sr}$ are the coupling added-mass matrices between the rigid-body and flexible velocity potentials, $\mathbf{M}_{rq}$ and $\mathbf{M}_{rs}$ are $6 \times 2N$ matrices, and $\mathbf{M}_{qr} = \mathbf{M}_{rq}^T$, $\mathbf{M}_{sr} = \mathbf{M}_{rs}^T$; $\mathbf{M}_{qq}$, $\mathbf{M}_{sq}$, $\mathbf{M}_{qs}$, and $\mathbf{M}_{ss}$ are the $2N \times 2N$ flexible added-mass matrices, and $\mathbf{M}_{sq} = \mathbf{M}_{qs}^T$.

We now explain the nature of the terms in the kinetic energy $\mathcal{T}_f$. If the deformation is zero, $\dot{\mathbf{q}} = \mathbf{q} = \mathbf{0}$, and the fluid's kinetic energy reduces to the first term $\mathcal{T}_f = \frac{1}{2}\boldsymbol{\upsilon}^T\mathbf{M}_{rr}\boldsymbol{\upsilon}$ which is the kinetic energy of a potential fluid in which a rigid-body vehicle is maneuvering. The second and third terms in Eq. (14) effectively represent the energy of

**Table 1 Added-mass matrix entities**

| Matrix | Entities | | |
|---|---|---|---|
| $\mathbf{M}_{rr}$ | $M_{rr,ij} = -\rho \iint_{S_B} \Phi_{ri} \frac{\partial \Phi_{rj}}{\partial n} \, dS$, | $i = 1, 2, \ldots, 6$, | $j = 1, 2, \ldots, 6$ |
| $\mathbf{M}_{rq}$ | $M_{rq,ij} = -\rho \iint_{S_B} \Phi_{ri} \frac{\partial \Phi_{qj}}{\partial n} \, dS$, | $i = 1, 2, \ldots, 6$, | $j = 1, 2, \ldots, 2N$ |
| $\mathbf{M}_{qr}$ | $M_{qr,ij} = -\rho \iint_{S_B} \Phi_{qi} \frac{\partial \Phi_{rj}}{\partial n} \, dS$, | $i = 1, 2, \ldots, 2N$, | $j = 1, 2, \ldots, 6$ |
| $\mathbf{M}_{qq}$ | $M_{qq,ij} = -\rho \iint_{S_B} \Phi_{qi} \frac{\partial \Phi_{qj}}{\partial n} \, dS$, | $i = 1, 2, \ldots, 2N$, | $j = 1, 2, \ldots, 2N$ |
| $\mathbf{M}_{rs}$ | $M_{rs,ij} = -\rho \iint_{S_B} \Phi_{ri} \frac{\partial \Phi_{sj}}{\partial n} \, dS$, | $i = 1, 2, \ldots, 6$, | $j = 1, 2, \ldots, 2N$ |
| $\mathbf{M}_{sr}$ | $M_{sr,ij} = -\rho \iint_{S_B} \Phi_{si} \frac{\partial \Phi_{rj}}{\partial n} \, dS$, | $i = 1, 2, \ldots, 2N$, | $j = 1, 2, \ldots, 6$ |
| $\mathbf{M}_{qs}$ | $M_{qs,ij} = -\rho \iint_{S_B} \Phi_{qi} \frac{\partial \Phi_{sj}}{\partial n} \, dS$, | $i = 1, 2, \ldots, 2N$, | $j = 1, 2, \ldots, 2N$ |
| $\mathbf{M}_{sq}$ | $M_{sq,ij} = -\rho \iint_{S_B} \Phi_{si} \frac{\partial \Phi_{qj}}{\partial n} \, dS$, | $i = 1, 2, \ldots, 2N$, | $j = 1, 2, \ldots, 2N$ |
| $\mathbf{M}_{ss}$ | $M_{ss,ij} = -\rho \iint_{S_B} \Phi_{si} \frac{\partial \Phi_{sj}}{\partial n} \, dS$, | $i = 1, 2, \ldots, 2N$, | $j = 1, 2, \ldots, 2N$ |

a $2N$-DOF spring-mass system associated with the elastic deformation, with a generalized added-mass matrix $\mathbf{M}_{qq}$ and a stiffness matrix $u_0^2\mathbf{M}_{ss}$. In particular, it has been demonstrated in the context of ship vibration that the generalized added-mass matrix $\mathbf{M}_{qq}$ can significantly reduce the natural vibration frequencies of a vehicle moving in a heavy fluid [25]. The other terms in Eq. (14) denote the kinetic energy due to the coupling between the rigid-body motion and elastic deformation.

### 3. Potential-Flow Aerodynamic Force Expressions

The potential-flow aerodynamic forces and moments can be derived from Kirchhoff's equation, and the corresponding elastic generalized forces can be derived from Lagrange's equation in terms of generalized coordinates. The results are summarized as follows.

To obtain a concise formulation for the aerodynamic force, moment, and generalized force, the $6 \times 6$ rigid-body added-mass matrix $\mathbf{M}_{rr}$ and the $6 \times 2N$ rigid-flexible coupling added-mass matrices $\mathbf{M}_{rq}$ and $\mathbf{M}_{rs}$ are written as

$$\mathbf{M}_{rr} = \begin{bmatrix} \mathbf{M}_{rr11} & \mathbf{M}_{rr12} \\ \mathbf{M}_{rr21} & \mathbf{M}_{rr22} \end{bmatrix}, \qquad \mathbf{M}_{rq} = \begin{bmatrix} \mathbf{M}_{rq1} \\ \mathbf{M}_{rq2} \end{bmatrix}, \qquad \mathbf{M}_{rs} = \begin{bmatrix} \mathbf{M}_{rs1} \\ \mathbf{M}_{rs2} \end{bmatrix} \tag{15}$$

where the matrices $\mathbf{M}_{rr11}, \mathbf{M}_{rr12}, \mathbf{M}_{rr21}$, and $\mathbf{M}_{rr22}$ are $3 \times 3$ matrices and $\mathbf{M}_{rq1}$, $\mathbf{M}_{rq2}$, $\mathbf{M}_{rs1}$, and $\mathbf{M}_{rs2}$ are $3 \times 2N$ matrices. With the preceding definitions, the potential-flow forces and moments can be obtained as

$$\begin{bmatrix} \mathbf{F}_P \\ \mathbf{M}_P \\ \mathbf{Q}_P \end{bmatrix} = -\begin{bmatrix} \mathbf{M}_{A11} & \mathbf{M}_{A12} & \mathbf{M}_{A13} \\ \mathbf{M}_{A21} & \mathbf{M}_{A22} & \mathbf{M}_{A23} \\ \mathbf{M}_{A31} & \mathbf{M}_{A32} & \mathbf{M}_{A33} \end{bmatrix} \begin{bmatrix} \dot{\mathbf{v}}_0 \\ \dot{\boldsymbol{\omega}} \\ \ddot{\mathbf{q}} \end{bmatrix} + \begin{bmatrix} \mathbf{F}_{P,\text{non}}(\mathbf{v}_0, \boldsymbol{\omega}, \mathbf{q}, \dot{\mathbf{q}}) \\ \mathbf{M}_{P,\text{non}}(\mathbf{v}_0, \boldsymbol{\omega}, \mathbf{q}, \dot{\mathbf{q}}) \\ \mathbf{Q}_{P,\text{non}}(\mathbf{v}_0, \boldsymbol{\omega}, \mathbf{q}, \dot{\mathbf{q}}) \end{bmatrix} \tag{16}$$

where the first term is related to the linear acceleration $\dot{\mathbf{v}}_0$, angular acceleration $\dot{\boldsymbol{\omega}}$, and the elastic generalized acceleration $\ddot{\mathbf{q}}$, whereas the second term contains nonlinear functions of the rigid-body velocities $\mathbf{v}_0$, $\boldsymbol{\omega}$, the generalized coordinate $\mathbf{q}$, and the generalized velocity $\dot{\mathbf{q}}$. The coefficient matrix in the first term, later abbreviated to $\mathbf{M}_{\text{AT}}$, is the $(6 + 2N) \times (6 + 2N)$ symmetric total added-mass matrix of the flexible airship. To incorporate the potential-flow aerodynamics, the first term is added to the left-hand side of the equations of motion (3), so that the mass matrix $\mathbf{M}_{\text{sys}}$ is replaced with $\mathbf{M}_{\text{sys}} + \mathbf{M}_{\text{AT}}$, while $\mathbf{F}_{P,\text{non}}$, $\mathbf{M}_{P,\text{non}}$, and $\mathbf{Q}_{P,\text{non}}$ are incorporated into the right-hand side of the equations of motion.

The total added-mass matrix can be written as the summation of four matrices as

$$\mathbf{M}_{\text{AT}} = \begin{bmatrix} \mathbf{M}_{rr} & \mathbf{M}_{rq} \\ \mathbf{M}_{qr} & \mathbf{M}_{qq} \end{bmatrix} + \begin{bmatrix} \mathbf{M}_{rs}\mathbf{q} & 0 & \cdots & 0 \\ \mathbf{M}_{qs}\mathbf{q} & 0 & \cdots & 0 \end{bmatrix} + \begin{bmatrix} \mathbf{q}^T\mathbf{M}_{sr} & \mathbf{q}^T\mathbf{M}_{sq} \\ 0 & 0 \\ \vdots & \vdots \\ 0 & 0 \end{bmatrix} + \begin{bmatrix} \mathbf{q}^T\mathbf{M}_{ss}\mathbf{q} & 0 & \cdots & 0 \\ 0 & 0 & \cdots & 0 \\ \vdots & \vdots & \vdots & \vdots \\ 0 & 0 & \cdots & 0 \end{bmatrix} \tag{17}$$

in which $\mathbf{q}^T\mathbf{M}_{sr}$ and $\mathbf{q}^T\mathbf{M}_{sq}$ are $1 \times 6$ and $1 \times 2N$ row vectors, respectively, $\mathbf{M}_{rs}\mathbf{q}$ and $\mathbf{M}_{qs}\mathbf{q}$ are $6 \times 1$ and $2N \times 1$ vectors, respectively, and $\mathbf{q}^T\mathbf{M}_{ss}\mathbf{q}$ is a scalar. The nonlinear force and moment terms are given as follows:

$$\begin{aligned} \mathbf{F}_{P,\text{non}} = {} & -\boldsymbol{\omega}^{\times}\mathbf{M}_{rr11}\mathbf{v}_0 - \boldsymbol{\omega}^{\times}\mathbf{M}_{rr12}\boldsymbol{\omega} - \boldsymbol{\omega}^{\times}\mathbf{M}_{rq1}\dot{\mathbf{q}} - u_0\boldsymbol{\omega}^{\times}\mathbf{M}_{rs1}\mathbf{q} \\ & - u_0\mathbf{M}_{rs1}\dot{\mathbf{q}} - [\boldsymbol{\upsilon}^T\mathbf{M}_{rs}\dot{\mathbf{q}} + \dot{\mathbf{q}}^T\mathbf{M}_{sq}\dot{\mathbf{q}} + 2u_0\dot{\mathbf{q}}^T\mathbf{M}_{ss}\mathbf{q}, 0, 0]^T \\ & - \boldsymbol{\omega}^{\times}[\boldsymbol{\upsilon}^T\mathbf{M}_{rs}\mathbf{q} + \mathbf{q}^T\mathbf{M}_{sq}\dot{\mathbf{q}} + u_0\mathbf{q}^T\mathbf{M}_{ss}\mathbf{q}, 0, 0]^T \end{aligned} \tag{18}$$

$$\begin{aligned} \mathbf{M}_{P,\text{non}} = {} & -\mathbf{v}_0^{\times}\mathbf{M}_{rr11}\mathbf{v}_0 - \mathbf{v}_0^{\times}\mathbf{M}_{rr12}\boldsymbol{\omega} - \boldsymbol{\omega}^{\times}\mathbf{M}_{rr21}\mathbf{v}_0 - \boldsymbol{\omega}^{\times}\mathbf{M}_{rr22}\boldsymbol{\omega} \\ & - \mathbf{v}_0^{\times}\mathbf{M}_{rq1}\dot{\mathbf{q}} - \boldsymbol{\omega}^{\times}\mathbf{M}_{rq2}\dot{\mathbf{q}} - u_0\mathbf{M}_{rs2}\dot{\mathbf{q}} - u_0\boldsymbol{\omega}^{\times}\mathbf{M}_{rs2}\mathbf{q} \\ & - \mathbf{v}_0^{\times}(u_0\mathbf{M}_{rs1}\mathbf{q} + [\boldsymbol{\upsilon}^T\mathbf{M}_{rs}\mathbf{q} + \mathbf{q}^T\mathbf{M}_{sq}\dot{\mathbf{q}} + u_0\mathbf{q}^T\mathbf{M}_{ss}\mathbf{q}, 0, 0]^T) \end{aligned} \tag{19}$$

$$\mathbf{Q}_{P,\text{non}} = -u_0\mathbf{M}_{qs}\dot{\mathbf{q}} + u_0\mathbf{M}_{sq}\dot{\mathbf{q}} + u_0^2\mathbf{M}_{ss}\mathbf{q} + u_0\mathbf{M}_{sr}\boldsymbol{\upsilon} \tag{20}$$

The first two terms in $\mathbf{F}_{P,\text{non}}$ and the first four terms in $\mathbf{M}_{P,\text{non}}$ are the force and moment terms due to the rigid-body motion, and, in particular, the first term in $\mathbf{M}_{P,\text{non}}$ is known as the Munk moment [26] which tends to destabilize the pitch and yaw rotations. The third term in $\mathbf{F}_{P,\text{non}}$ and the fifth and sixth terms in $\mathbf{M}_{P,\text{non}}$ are due to the coupling between the deflection rates and rigid-body motion, and the other terms in $\mathbf{F}_{P,\text{non}}$ and $\mathbf{M}_{P,\text{non}}$ are related to the bending slopes. The first two terms in $\mathbf{Q}_{P,\text{non}}$ denote the aerodynamic damping effects on the elastic deformation; the term $u_0^2\mathbf{M}_{ss}\mathbf{q}$ is an effective aerodynamic stiffness term, and the last term represents the influence of the rigid-body motion on the deformation.

To compute the total added-mass matrix $\mathbf{M}_{\text{AT}}$, the matrices defined in Table 1 must be evaluated. The added-mass matrix related to the pure rigid-body motion $\mathbf{M}_{rr}$ can be computed with the approach discussed in [7]. For the other added-mass matrices, $\mathbf{M}_{rq}$, $\mathbf{M}_{qr}$, $\mathbf{M}_{qq}$, $\mathbf{M}_{rs}$, $\mathbf{M}_{sr}$, $\mathbf{M}_{qs}$, $\mathbf{M}_{sq}$, and $\mathbf{M}_{ss}$, the Laplace equations must be solved to obtain $\Phi_{ri}$, $\Phi_{qi}$, and $\Phi_{si}$; then, the elements of each added-mass matrix can be evaluated by the integrals defined in Table 1. In this work, the analytical solution of the Laplace equation for an ellipsoid of revolution [24,25] is applied to obtain $\Phi_{ri}$, $\Phi_{qi}$, and $\Phi_{si}$ and to compute the added-mass matrices. The readers are referred to [27] for a detailed description of the computational procedure. Once the added-mass matrices are computed, the potential-flow aerodynamic force and moment can be obtained from Eqs. (16–20).

### B. Viscous Effect on the Hull

Wind-tunnel tests on the aerodynamics of bodies of revolution at nonzero angles of attack have shown that a prediction based on a potential-flow assumption can cause considerable error because of the effects of viscosity, especially at the rear of the body. A semi-empirical estimation approach has been applied to rigid-body airships, in which the viscous effect on the hull starts from a position $\varepsilon_V$ along the hull [7]. To extend this method for an elastic airship, the corresponding aerodynamic normal force distribution along the centerline is first predicted using the local velocity of a deformed airship, that is,

$$\mathbf{f}_V = f_{VN}\left[0, \frac{-v_{V,d}}{\sqrt{v_{V,d}^2 + w_{V,d}^2}}, \frac{-w_{V,d}}{\sqrt{v_{V,d}^2 + w_{V,d}^2}}\right]^T, \quad \text{from } \varepsilon_V \text{ to the end} \tag{21}$$

where

$$f_{VN} = -q_0(k_2 - k_1)\sin 2\gamma \cdot \frac{\mathrm{d}S}{\mathrm{d}\varepsilon} + q_0 \eta C_{\mathrm{DC}} \sin^2\gamma \cdot 2R$$

in which $k_1$ and $k_2$ are added-mass factors [7], $\eta$ is an efficiency factor accounting for the finite length of the hull [7], $C_{\mathrm{DC}}$ is the crossflow drag [7], and $R$ is the hull's cross-sectional radius. The first term in $f_{VN}$ effectively removes the inviscid flow contribution, while the second term replaces it with a viscous flow contribution. The velocity components $u_{V,d}$, $v_{V,d}$, and $w_{V,d}$ denote the local velocity at the position $\varepsilon_V$ on a deformed airship computed using Eq. (11). These velocity components are also used to compute the dynamic pressure $q_0$ and the angle between centerline and velocity vector $\gamma$ for a flexible airship as shown in Fig. 3, that is,

$$\gamma = \tan^{-1}\left(\frac{\sqrt{v_{V,d}^2 + w_{V,d}^2}}{u_{V,d}}\right) \tag{22}$$

The total viscous force and moment on the hull can be readily computed by integrating $\mathbf{f}_V$ and $(\mathbf{r} + \mathbf{u})^{\times}\mathbf{f}_V$ from $\varepsilon_V$ to the end of the hull, respectively. Unlike the rigid-body model, the resulting roll moment is not zero for a flexible airship due to the term $\mathbf{u}^{\times}\mathbf{f}_V$. The moment arm $\mathbf{u}$ reflects the deflection of the centerline from the $x$ axis of the undeformed airship, as shown in Fig. 1. The elastic generalized force of the $i$th shape function is computed as

$$Q_{Vi} = \int_{\varepsilon_V}^{L} \mathbf{f}_V^T \boldsymbol{\Psi}\, \mathrm{d}\varepsilon$$

Substituting $\mathbf{f}_V$ from Eq. (21), we have

$$Q_{Vi} = [-q_0(k_2 - k_1)\sin 2\gamma \cdot \mathbf{I}_{V1,i}^T + q_0 \eta C_{\mathrm{DC}} \sin^2\gamma \cdot \mathbf{I}_{V2,i}^T]\left[0, \frac{-v_{V,d}}{\sqrt{v_{V,d}^2 + w_{V,d}^2}}, \frac{-w_{V,d}}{\sqrt{v_{V,d}^2 + w_{V,d}^2}}\right]^T \tag{23}$$

Two new shape function integrals are employed in Eq. (23),

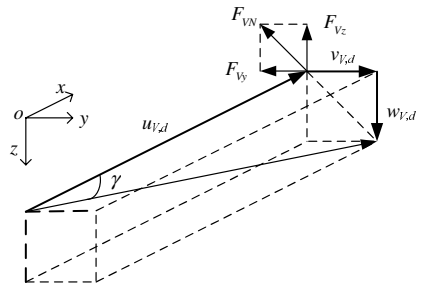


**Fig. 3 Angle between centerline and velocity vector.**

$$\mathbf{I}_{V1,i} = \int_{\varepsilon_V}^{L} \frac{\mathrm{d}S}{\mathrm{d}\varepsilon}\boldsymbol{\Psi}_{\mathbf{i}}\, \mathrm{d}\varepsilon, \qquad \mathbf{I}_{V2,i} = \int_{\varepsilon_V}^{L} 2R\boldsymbol{\Psi}_{\mathbf{i}}\, \mathrm{d}\varepsilon \tag{24}$$

We can see that the influence of the flexibility on the viscous effect is incorporated through the local velocity components $u_{V,d}$, $v_{V,d}$, and $w_{V,d}$ in the computation of the dynamic pressure and the angle $\gamma$, as well as by adding a roll moment related to the centerline deflection.

### C. Force Acting on the Fins

We now turn our attention to the force produced by the fins, normal to the airship centerline. This is obtained by estimating the force distribution and integrating it over the fin area. The fin force per unit length can be computed as $\mathbf{f}_F = f_{FN}[0, \cos\Phi_F, -\sin\Phi_F]^T$, where $\Phi_F$ is the angle from the $oxz$ plane to the fin plane as shown in Fig. 4, and [7]

$$f_{FN} = q_0 \frac{C_{L\alpha}}{C_{l\alpha}} \alpha_F \int_R^b \Delta C_{p\alpha}(x, s)\left(1 + \frac{R^2}{s^2}\right) \mathrm{d}s \tag{25}$$

in which $\Delta C_{p\alpha} \equiv \partial \Delta C_p / \partial\alpha$, and $\Delta C_p$ is the pressure coefficient of the airfoil, $C_{L\alpha}$ and $C_{l\alpha}$ are the 3-D and 2-D lift curve slopes of the fin, and $b$ is the fin's semispan, as shown in Fig. 5. The factor $(1 + R^2/s^2)$ accounts for the influence of the hull on the fins. For a flexible airship, the geometric angle of attack $\alpha_F$ used in the evaluation of $f_{FN}$ is computed with the velocity component $u_d(c/4)$ in the centerline direction and the component $v_{nd}(c/4)$ perpendicular to the fin surface at the center of the quarter-chord, where the subscript $d$ denotes the local velocity components on a deformed airship computed from Eq. (11), that is,

$$\alpha_F = \tan^{-1}\left[\frac{v_{nd}(c/4)}{u_d(c/4)}\right] \tag{26}$$

The total normal force and moment on the fin can then be obtained by integrating $\mathbf{f}_F$ and $(\mathbf{r} + \mathbf{u})^{\times}\mathbf{f}_F$ over the fin region, respectively. Again, an additional roll moment exists due to the term $\mathbf{u}^{\times}\mathbf{f}_V$. The elastic generalized force is computed as

$$Q_{Fi} = \int_{x_{Fs}}^{x_{Fe}} \mathbf{f}_F^T \boldsymbol{\Psi}_i\, \mathrm{d}x$$

or,

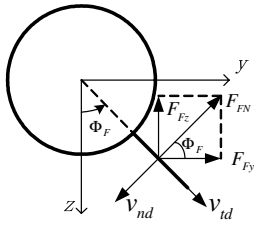


**Fig. 4 Normal force on a fin.**

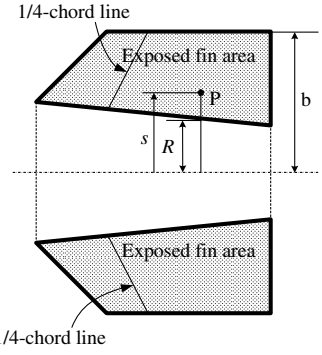


**Fig. 5 Fin planform.**

$$Q_{Fi} = q_0 \frac{C_{L\alpha}}{C_{l\alpha}} \alpha_F \mathbf{I}_{Fi}^T [0, \cos\Phi_F, -\sin\Phi_F]^T, \qquad i = 1, 2, \ldots, 2N \tag{27}$$

The shape function integrals $\mathbf{I}_{Fi}$ required in Eq. (27) are defined as

$$\mathbf{I}_{Fi} = \int_{x_{Fs}}^{x_{Fe}} \int_R^b \Delta C_{p\alpha}(x, s) \left(1 + \frac{R^2}{s^2}\right) \boldsymbol{\Psi}_i \, \mathrm{d}s \, \mathrm{d}x \tag{28}$$

in which $x_{Fs}$ and $x_{Fe}$ are the $x$ coordinates of the start and end positions of the fins. We can see that the influence of the flexibility on the fin forces is incorporated through the local velocity components $v_{nd}(c/4)$ and $u_d(c/4)$ for the computation of the geometric angle of attack $\alpha_F$, as well as an additional roll moment due to the deflection of the centerline from the $x$ axis of the undeformed airship.

### D. Force Acting on the Hull Due to the Fins

Based on the results from wind-tunnel tests on the aerodynamics of model airships, such as the Akron [28], it has been found that the presence of the fins can lead to an additional normal force on the hull, due to the fin-induced downwash over the airflow near the hull. The external force per unit length on the hull due to the fins can be obtained as $\mathbf{f}_{H(F)} = f_{H(F)}[0, \cos\Phi_F, -\sin\Phi_F]^T$, where $f_{H(F)} = 2q_0\alpha_F \pi R^2 C_{H(F)}$ and

$$C_{H(F)} = \frac{C_{L\alpha}}{C_{l\alpha}} \frac{\mathrm{d}}{\mathrm{d}x} \int_{x_{Fs}}^{x_{Fe}} \int_R^b [8\pi d_F (d_F - x + x_F)]^{-1} \times \Delta C_{p\alpha} \left(1 + \frac{R^2}{s^2}\right) \mathrm{d}s \, \mathrm{d}x_F \tag{29}$$

where $d_F = \sqrt{(x - x_F)^2 + s^2}$. For a flexible airship, $f_{H(F)}$ should be computed with the angle of attack $\alpha_F$ from Eq. (26). The corresponding total force and external moment are computed by integrating $\mathbf{f}_{H(F)}$ and $(\mathbf{r} + \mathbf{u})^\times \mathbf{f}_{H(F)}$ over the hull, respectively, and the elastic generalized force is computed as

$$Q_{H(F),i} = 2q_0\alpha_F \mathbf{I}_{H(F),i}^T [0, \cos\Phi_F, -\sin\Phi_F]^T, \qquad i = 1, 2, \ldots, 2N \tag{30}$$

The new shape function integrals $\mathbf{I}_{H(F),i}$ employed in Eq. (30) are defined as

$$\mathbf{I}_{H(F),i} = \int_L \pi R^2 C_{H(F)} \boldsymbol{\Psi}_i \, \mathrm{d}x$$

Similar to the fin forces, the influence of the flexibility on $\mathbf{F}_{H(F)}$ and $\mathbf{M}_{H(F)}$ is incorporated through the local velocity in the computation of the geometric angle of attack, as well as an additional roll moment due to the deflection of the centerline.

### E. Axial Drag

The axial drag force acting on the hull and on a fin are modeled as concentrated forces at the c.v. and at the center of the fin's quarter-chord, respectively. The external axial drag forces $\mathbf{F}_{\text{axial},H}$ and $\mathbf{F}_{\text{axial},F}$ can be computed using the method presented in [7], with the dynamic pressure and the local angles of attack at the c.v. and at the center of the fin's quarter-chord calculated from the velocity components in Eq. (11). In addition, the elastic displacement should be considered in the moment computation, so that the moments due to the axial drag on the hull and on a fin are

$$\begin{aligned} \mathbf{M}_{\text{axial},H} &= \sum_{i=1}^{2N} q_i(t) \mathbf{I}_{\text{AS},i}^\times \mathbf{F}_{\text{axial},H} \\ \mathbf{M}_{\text{axial},F} &= \mathbf{r}(c/4)^\times \mathbf{F}_{\text{axial},F} + \sum_{i=1}^{2N} q_i \boldsymbol{\Psi}_i(c/4)^\times \mathbf{F}_{\text{axial},F} \end{aligned} \tag{31}$$

where

$$\sum_{i=1}^{2N} q_i(t) \mathbf{I}_{\text{AS},i}$$

is the elastic displacement of the c.v., $\mathbf{r}(c/4)$ denotes the position vector of the center of quarter-chord from the body-frame origin on the undeformed airship, and $\boldsymbol{\Psi}_i(c/4)$ is the $i$th shape function at this point. Because the axial drag is along the $x$ axis, whereas the modeled flexibility is due to bending only, the corresponding elastic forces are zero, that is, $Q_{\text{axial},Hi} = Q_{\text{axial},Fi} = 0$.

### F. Force and Moment Due to Control Surface Deflection

The force due to the control surface deflection is modeled as a concentrated force acting at a position $\mathbf{r}_\delta$ on the undeformed body. The external force $\mathbf{F}_\delta$ and the position $\mathbf{r}_\delta$ can be computed using the methods presented in [7]. The external moment due to the control surface deflection is calculated as

$$\mathbf{M}_\delta = \mathbf{r}_\delta^\times \mathbf{F}_\delta + \sum_{i=1}^{2N} q_i(t) \boldsymbol{\Psi}_i(\mathbf{r}_\delta)^\times \mathbf{F}_\delta \tag{32}$$

The second term reflects the fact that the elastic deflection at $\mathbf{r}_\delta$ should be incorporated in the moment arm when computing the external moment. The elastic force due to the control surface deflection is then obtained as $Q_{\delta i} = \mathbf{F}_\delta^T \boldsymbol{\Psi}_i(\mathbf{r}_\delta)$. Finally, the rudder and elevator forces and moments $\mathbf{F}_\delta$, $\mathbf{M}_\delta$, and $\mathbf{Q}_\delta$ are included in $\mathbf{F}_C$, $\mathbf{M}_C$, and $\mathbf{Q}_C$, respectively, in the equations of motion (3).

Incorporating all the inertial, gravitational, thrust, aerostatic, and aerodynamic forces into the equations of motion (3) completes the dynamics model of a flexible airship.

## IV. Simulation Results

### A. Simulated Airship

A dynamics simulation program was developed in the MATLAB environment to implement the nonlinear dynamics model [27]. The solution of the equations of motion for a flexible airship requires its geometry, inertial properties, and bending stiffness distribution. In the numerical simulations presented here, the Skyship-500 nonrigid airship (shown in Fig. 6) is used as an example because its geometric and inertial parameters (mass, inertia tensor, and position of c.g.) are available in [3,7]. We consider a neutrally buoyant Skyship-500, with an air density of $\rho = 1.158$ kg/m$^2$ and a maximum operating flight speed of 30 m/s.

The variation of mass per unit length $\bar{m}$ along the centerline was estimated from a CAD model based on the inertial information from [3] and is plotted in Fig. 7. If the internal pressure of the hull is high enough to prevent wrinkling, the bending stiffness $EI$ is calculated as $EI = \pi R^3 ET$, where $R$ is the cross-sectional radius of the hull, $E$ is the elastic modulus of the hull envelope, and $T$ is its thickness. The envelope material properties were not provided for the Skyship-500 in [3], and thus the bending stiffness used in the simulation is computed from the material properties of the fabric in [10],

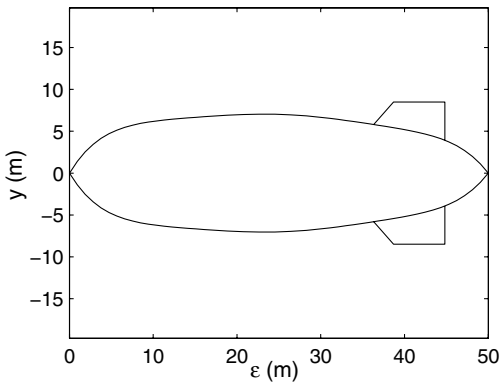


**Fig. 6 Skyship-500 airship ($\varepsilon$: distance from the nose).**

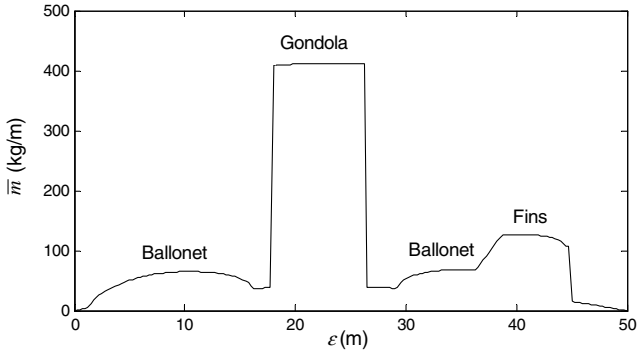


**Fig. 7 Mass per unit length of the Skyship-500.**

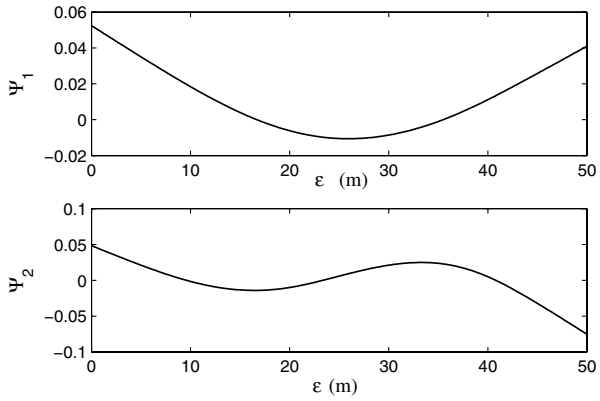


**Fig. 8 First two normal mode shapes.**

specifically, for $ET = 433,440$ N/m. This value was measured with biaxial stress cylinder tests for the envelopes of two aerostats [10].

In this work, two shape functions are employed to describe the deflections of the Skyship-500 airship in each of the lateral and longitudinal planes, that is, $N = 2$ and the generalized elastic coordinate vector is written as $\mathbf{q} = [q_1, q_2, q_3, q_4]^T$, where $q_1$ and $q_2$ describe the bending deformation in the lateral plane, whereas $q_3$ and $q_4$ represent the deformation in the longitudinal plane. The two mode shapes $\Psi_1$ and $\Psi_2$ are plotted in Fig. 8 and the corresponding natural frequencies are $\omega_{n1} = 22.8$ rad/s and $\omega_{n2} = 64.2$ rad/s.

### B. Generalized Added-Mass Matrix

We now investigate the influence of potential-flow aerodynamic force on the vibration of the hull. Other researchers have demonstrated that the generalized added-mass matrix can significantly reduce the natural frequencies of a vehicle moving in a heavy fluid, such as a ship [25]. The generalized added-mass matrix $\mathbf{M}_{qq}$ of the Skyship-500 is calculated as

$$\mathbf{M}_{qq} = \begin{bmatrix} 0.75 & -0.14 & 0 & 0 \\ -0.14 & 0.96 & 0 & 0 \\ 0 & 0 & 0.75 & -0.14 \\ 0 & 0 & -0.14 & 0.96 \end{bmatrix}$$

This is compared to the $4 \times 4$ elastic generalized mass matrix $\mathbf{M}_{33}$, which is an identity matrix because of the orthogonality of the natural modes. We can see that the diagonal components in $\mathbf{M}_{qq}$ will considerably decrease the natural frequencies of the free vibrations. The resulting natural frequencies of the Skyship-500 in air are $\omega_{n1} = 17.2$ rad/s and $\omega_{n2} = 46.0$ rad/s, approximately 25–30% lower than those in vacuum, as given in Sec. IV.A.

### C. Time Responses

We now present the time responses to simple steplike inputs from the elevator and rudder. The response results for a flexible airship are compared with those computed from the dynamics model of a rigid-body vehicle as described in [7]. To perform the nonlinear dynamics simulation for a flexible airship, we first define the initial values of the motion states and control input. As an initial condition, the airship is in a steady level flight, that is, we define a steady-state forward speed $\bar{u}_0$. The airship experiences some static deformation $\bar{\mathbf{q}}$ due to gravity and aerostatic forces. All the other steady velocity components, $\bar{w}_0$ $\bar{v}_0$, $\bar{\boldsymbol{\omega}}$, and $\dot{\bar{\mathbf{q}}}$, are defined as zero at the initial time $t = 0$. Substituting the initial motion states into equations of motion (3) and setting the right-hand side of the equations to zero, we can obtain the initial control input ($\bar{\mathbf{F}}_C$, $\bar{\mathbf{M}}_C$, and $\bar{\mathbf{Q}}_C$) needed to maintain the steady level flight condition.

#### 1. Case 1: Response to Elevator Input

In this example, the initial steady level flight speed is $\bar{u}_0 = 30$ m/s, which is a high operating speed for the Skyship-500. The elevator deflection input $\delta_E$ (positive trailing edge downward) consists of a step input of 10 deg. The time histories of the linear and angular velocities in the longitudinal plane ($u_0$, $w_0$, $q$) and the corresponding aerodynamic forces and moment ($F_{\mathrm{AD},x}$, $F_{\mathrm{AD},z}$, $M_{\mathrm{AD},y}$) are displayed in Fig. 9 for both the rigid-body and flexible-body models of the airship. The time responses of the generalized coordinates and rates of the third and fourth modes (representing the deformation in the longitudinal plane) are drawn in Fig. 10. We can observe small effects of structural flexibility on the rigid-body motion and aerodynamic forces and moment in this maneuver. The oscillation frequencies of $\dot{q}_3$ and $\dot{q}_4$ are in agreement with the natural frequencies of the airship in air obtained in Sec. IV.B. These deflection rates are aerodynamically damped out in about 10 s.

#### 2. Case 2: Response to Rudder Input

In the second example, we specify a step rudder input $\delta_R$ of 10 deg (positive trailing edge left). Note that a proportional controller must be applied to the thrust input for the airship to maintain a constant airspeed. The rigid-body velocities ($v_0$, $p$, $r$) and aerodynamic force and moments ($F_{\mathrm{AD},y}$, $M_{\mathrm{AD},x}$, $M_{\mathrm{AD},z}$) in the lateral plane are shown in Fig. 11. The elastic generalized coordinates and rates are plotted in Fig. 12.

The effects of flexibility on the time histories of rigid-body velocities are minor in this example. Small differences between the flexible and rigid-body dynamics models can be observed in the yaw moment results. The sway speed $v_0$ in this case is higher than the heave speed $w_0$ in case 1 and causes more aerodynamic damping effects on the elastic motion. Therefore, the elastic generalized velocities are damped faster than those in case 1. The oscillation frequencies observed in the $\dot{q}_1$, $\dot{q}_2$ plots are slightly different from those in the $\dot{q}_3$, $\dot{q}_4$ plots in case 1, due to the coupling between the bending deformation in the lateral plane and the roll rotation. This coupling results from the fact that the c.g. of the airship is below the centerline.

### D. Frequency Response

A linear dynamics model is now formulated to investigate the frequency response to control inputs of the airship. For this purpose, we first introduce a reference equilibrium state $\overline{\mathbf{X}}$, about which the system will be linearized, and the corresponding control $\overline{\mathbf{U}}$, and then write the equations for the small disturbance from equilibrium as $\Delta\dot{\mathbf{X}} \approx \mathbf{A} \cdot \Delta\mathbf{X} + \mathbf{B} \cdot \Delta\mathbf{U}$, where the state matrix $\mathbf{A}$ and control input matrix $\mathbf{B}$ are evaluated numerically using finite difference of the nonlinear equations of motion. This linearization method has been applied to other nonlinear dynamics models for control design [29]. Once the state and input matrices are obtained, the responses in the frequency domain can be computed. The frequency responses of pitch and yaw rates due to elevator and rudder inputs at 30 m/s are displayed in Bode plots in Fig. 13. In addition, the response results from the rigid-body dynamics model of [7] are included for comparison.

We can observe the following:

1) The flexible and rigid-body models lead to similar results at low frequencies for both longitudinal and lateral motions, because the

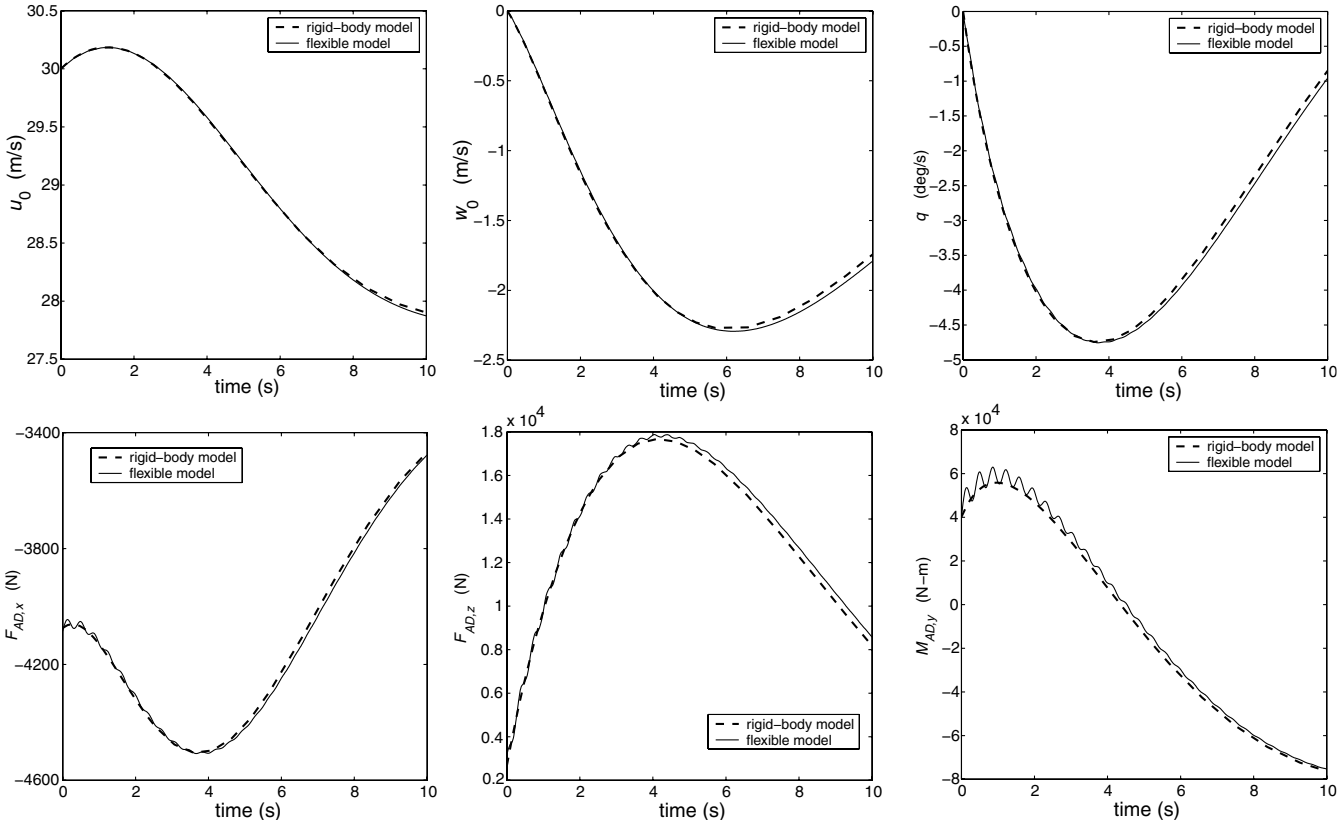


**Fig. 9 Time histories of rigid-body velocities, aerodynamic force, and moment, case 1, at 30 m/s.**

natural frequencies of elastic vibrations are much higher than those of rigid-body modes.

2) The differences between the rigid-body and flexible models occur at the natural frequencies of the Skyship-500 airship in air. However, even if excited at those natural frequencies, there is only a small amplification of the response due to high aerodynamic damping.

3) The influence of flexibility on the yaw rate $r$ is significantly stronger than that on the pitch rate $q$.

4) The natural frequencies observed in the yaw-rate plots are slightly different from those in the pitch-rate plots, because the elastic deflection in the lateral plane has strong coupling with the roll rotation, as discussed previously.

Although the flexibility effects turn out to be rather minor for the Skyship-500 airship, these effects could be significant in a case where the flexible natural frequencies are lower, for example if the airship were constructed of thinner materials.

## V. Aeroelastic Stability

We now investigate the possibility of whether the structural deformation of an airship can lead to instability of the rigid-body or elastic motion. Unlike the divergence or flutter analysis of a cantilevered wing of an airplane, the study here is based on the bending deformation of the hull of an airship and not its fins, not only because the hull is the largest flexible component of a modern airship, but also because the most important aerodynamic effect, the Munk moment [26], acts on the hull. We demonstrate that some rigid-body modes of an elastic airship can become unstable because the bending deflection reduces the effectiveness of the fins. The aeroelastic

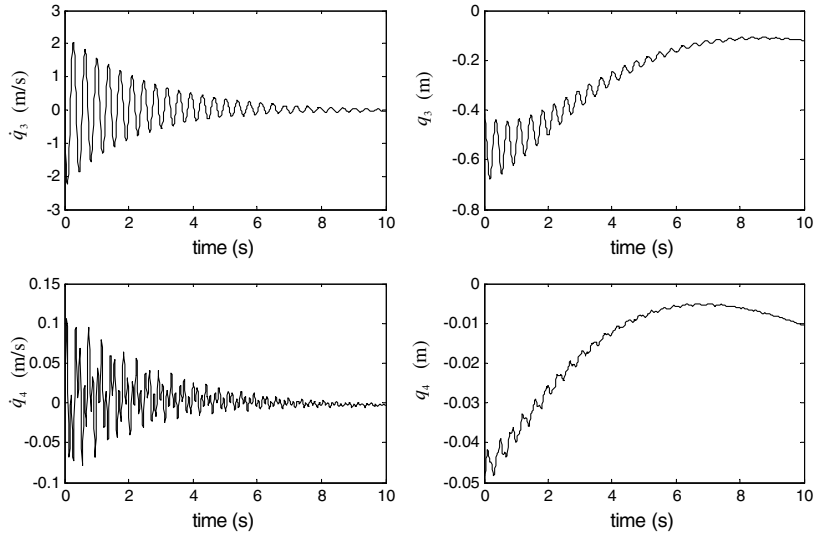


**Fig. 10 Time histories of generalized coordinates and velocities (case 1).**

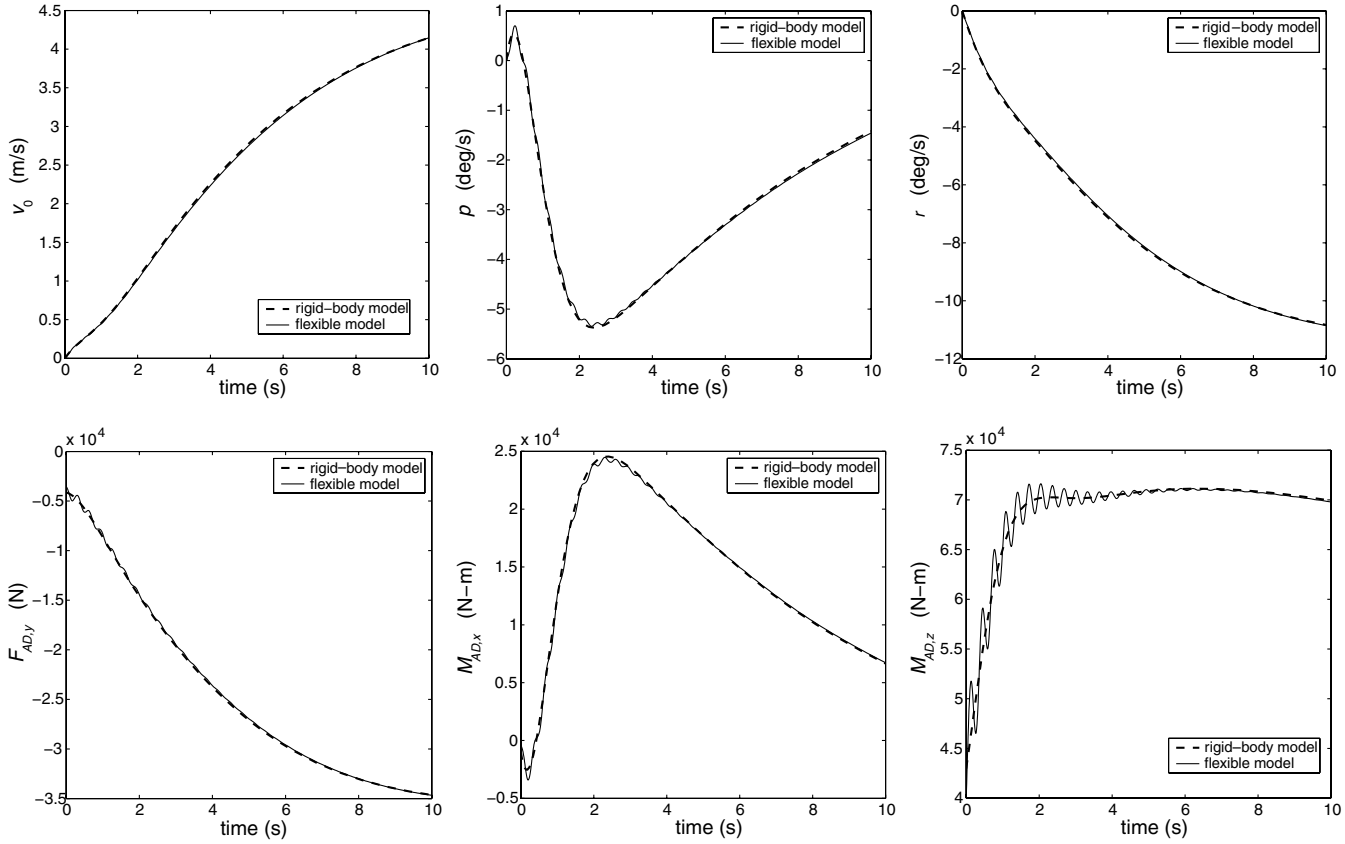


**Fig. 11 Time histories of rigid-body velocities, aerodynamic force and moment, case 2, at 30 m/s.**

instability of an airship is found to be similar to that of a slender missile, because it reflects the interaction of the vehicle's aerodynamics, elasticity, and flight dynamics. It has been found in [17] that the instability of a missile is associated with the interaction between its bending, aerodynamic force, and rigid-body motion (especially the roll rotation).

For the purpose of the stability analysis conducted here, the nonlinear model is linearized numerically, as discussed previously in Sec. IV.D. The variation of eigenvalues of the state matrix is calculated with airship forward speed. Once the real part of any eigenvalue becomes positive, aeroelastic instability occurs. This method is applied to analyze the stability of the Skyship-500 based on three dynamics models: the rigid-body model [7], the full flexible model represented by Eq. (3), and a simplified flexible model including only static deformation.

### A. Stability from the Rigid-Body Model

The eigenvalue results based on the rigid-body dynamics model are represented with the plots of real part $\sigma$ and imaginary part $\omega_d$ in Figs. 14 and 15. We can see that the longitudinal and lateral modes based on the rigid-body assumption are stable for all the speeds studied (0–130 m/s). The characteristics of each mode can be revealed by inspecting the eigenvectors corresponding to each eigenvalue. In particular, in the longitudinal plane, the first rigid-body mode is associated with the surge motion caused by aerodynamic axial drag, the second rigid-body mode is due to the coupling between the heave and pitch motion, and the third is a pitch-incidence oscillation mode [7]. In the lateral plane, the first and second lateral rigid-body modes are associated with the coupling sideslip-yaw and yaw-roll motion, respectively, and the third is a roll oscillation mode [7].

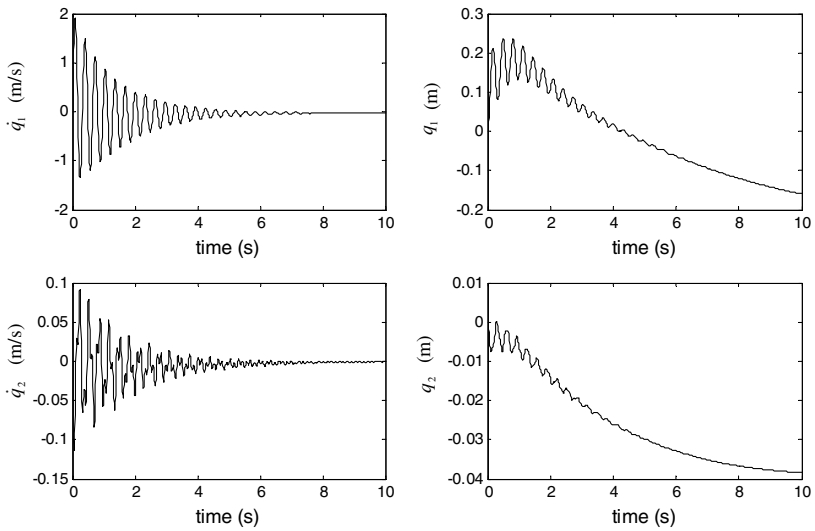


**Fig. 12 Time histories of generalized coordinates and velocities (case 2).**

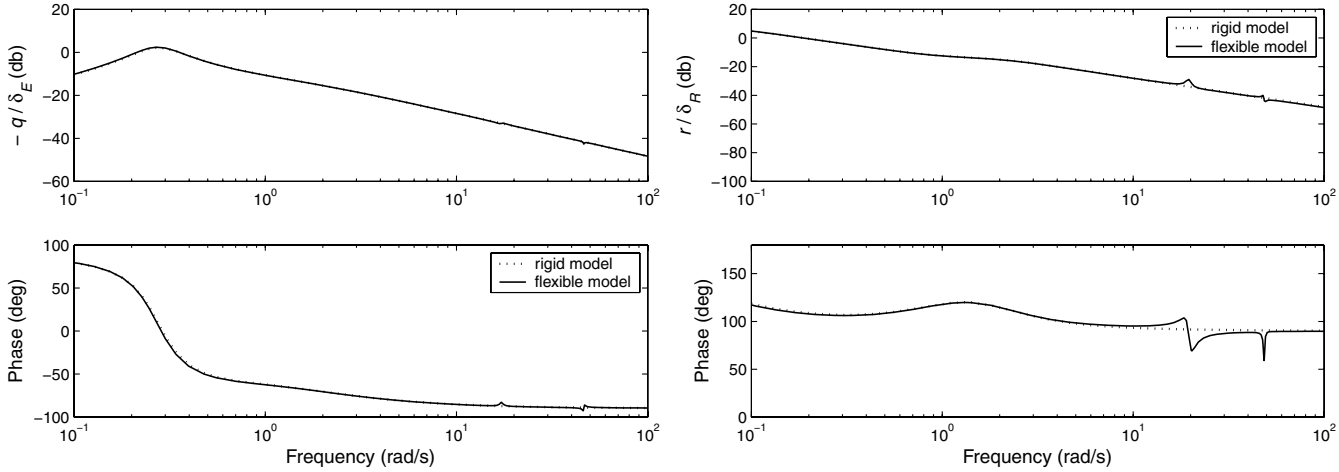


**Fig. 13 Control response in the frequency domain at 30 m/s.**

### B. Stability from the Full Flexible Model

The eigenvalue results from the flexible dynamics model in Eq. (3) for the longitudinal and lateral modes are displayed, respectively, in Figs. 16 and 17. From Fig. 16, we observe that an aeroelastic instability occurs at approximately 88 m/s, and we find that the third longitudinal rigid-body mode, related to pitch-incidence oscillation, becomes unstable ($\sigma > 0$ and $\omega_d > 0$) at this speed. The elements of the eigenvector of the corresponding unstable eigenvalue are dominated by a positive heave velocity $\Delta w_0$ (downward) and a negative third generalized coordinate $\Delta q_3$ (hull deflecting upward at both ends). That is, the third rigid-body mode becomes a pitch/bending coupling mode for an elastic airship. The cause of the aeroelastic instability is illustrated in Fig. 18. The vertical downward velocity $\Delta w_0$ leads to a nose-up unstable Munk moment and also generates three upward forces, $F_{V,z}$, $F_{F,z}$, and $F_{H(F),z}$, at the rear of the airship. The latter three aerodynamic forces result from the hull viscous effect, the force on the fins, and the force on the hull due to the fins, respectively, and they produce nose-down pitching moments which tend to stabilize the airship. However, the upward deflection at the rear causes a decrease in the local angles of attack, which effectively produces three downward forces $\Delta F_{V,z}$, $\Delta F_{F,z}$, and $\Delta F_{H(F),z}$. In other words, the deformation reduces the stabilizing aerodynamic effects of viscosity and fin force. As the forward speed increases to 88 m/s, $\Delta F_{V,z}$, $\Delta F_{F,z}$, and $\Delta F_{H(F),z}$ become significant,

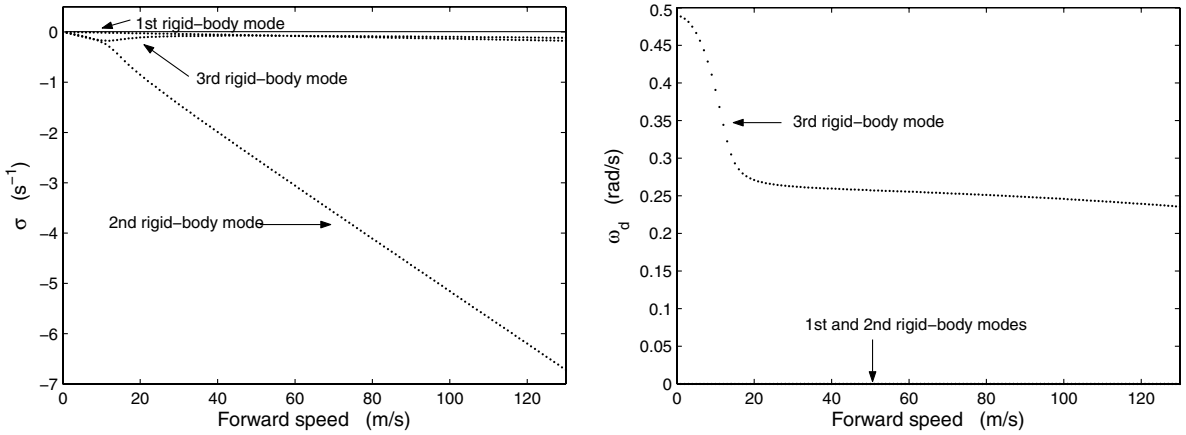


**Fig. 14 Eigenvalues of longitudinal modes from rigid-body dynamics.**

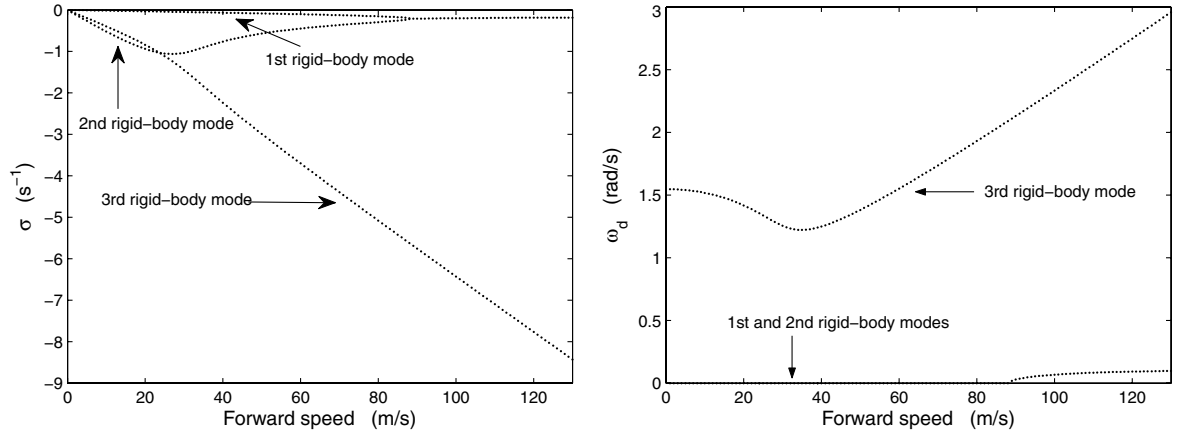


**Fig. 15 Eigenvalues of lateral modes from rigid-body dynamics.**

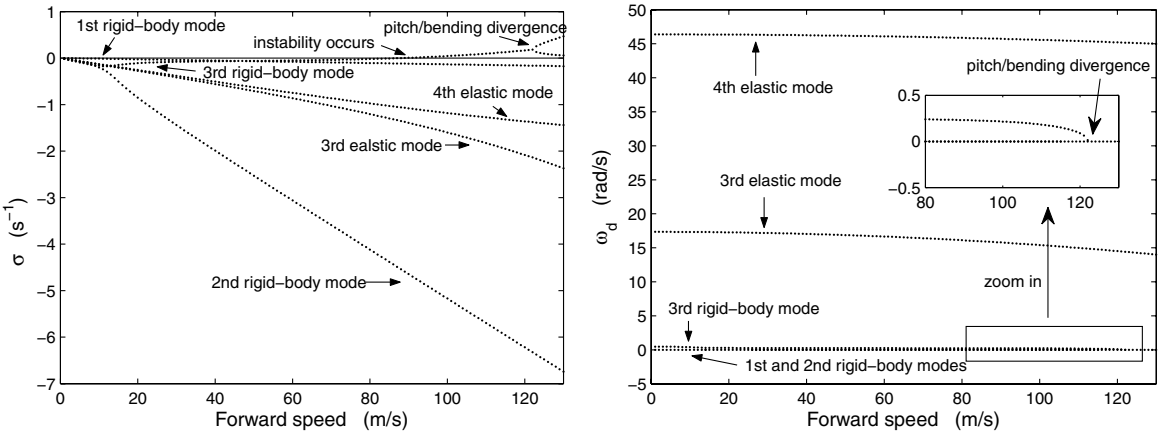


**Fig. 16 Eigenvalues of longitudinal modes from flexible-body dynamics.**

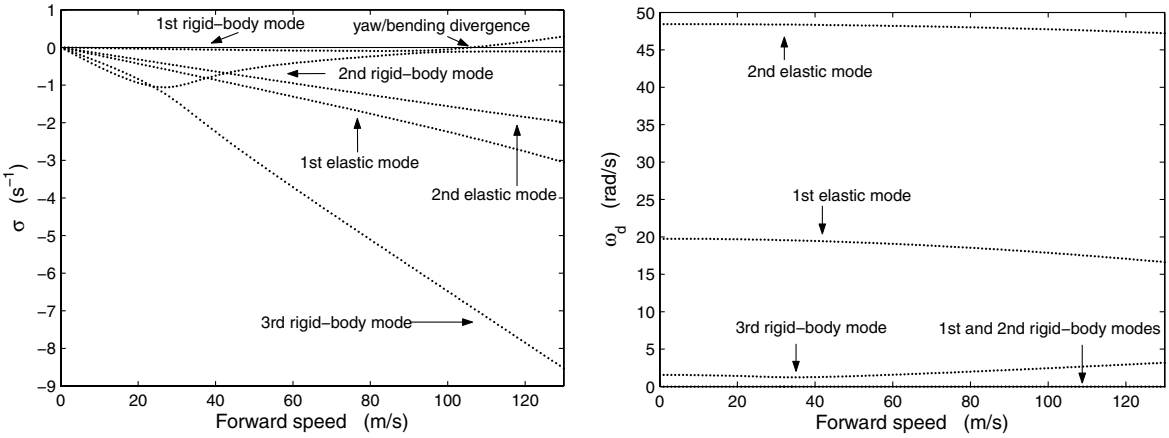


**Fig. 17 Eigenvalues of lateral modes from flexible-body dynamics.**

so that the viscous effect and the fin force cannot provide enough negative pitch moment to stabilize the airship. The positive imaginary part $\omega_d$ of the eigenvalue indicates that the system exhibits an underdamped oscillation. As the speed increases to 123 m/s, the deformation further reduces the stable aerodynamic effects, so that the real part of the eigenvalue $\sigma$ becomes more positive and the imaginary part $\omega_d$ becomes zero for this mode, representing that pitch/bending divergent instability occurs.

From Fig. 17, the first lateral rigid-body mode, related to sideslip-yaw motion, becomes divergent at about 106 m/s. Inspection of the corresponding eigenvector reveals that this rigid-body mode becomes a yaw/bending coupling mode for an elastic airship. This instability is caused by the yaw Munk moment and by the decrease of the aerodynamic damping effects due to the bending deflection in the lateral plane. Note that there are no oscillatory instabilities that can be observed in the lateral motion, because the Munk moment has small influence on the third lateral rigid-body mode, which is a roll oscillation.

The aeroelastic instability discussed here reflects the interaction between the aerodynamics, deformation, and rigid-body motion of the airship. The generation of this instability results from the existence of the unstable aerodynamic Munk moment and from the fact that the deformation reduces the other aerodynamic effects that stabilize the airship. For the Skyship-500, the operating flight speed is usually less than half of the lowest aeroelastic instability speed determined here. However, a different construction, with lower $ET$, could conceivably bring the aeroelastic instability into the operational regime of the airship.

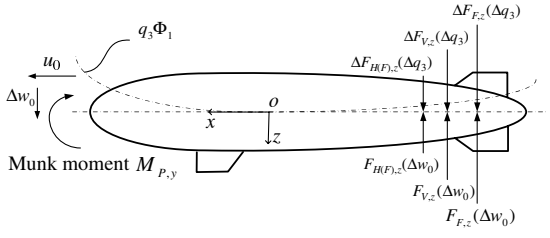


**Fig. 18 Cause of the aeroelastic instability.**

### C. Stability from a Simplified Flexible Model

The frequency response analysis in Sec. IV and the stability analysis presented here indicate that the natural frequencies of elastic vibrations are much higher than those of rigid-body modes. Therefore, it could be argued that the dynamic flexibility effects may be neglected in the aeroelastic analysis. In this subsection, we investigate the possibility of using a simplified flexible model to predict the instability speed of the Skyship-500. In particular, we neglect the dynamic flexibility effects and the influence of deformation on the inertial, gravitational, aerostatic, and control terms, and only incorporate the static deformation into the aerodynamic force and moment in the rigid-body dynamics model. The resulting quasi-static model can be represented as

$$\begin{bmatrix} \mathbf{M}_{11} & \mathbf{M}_{12} \\ \mathbf{M}_{21} & \mathbf{M}_{22} \end{bmatrix} \begin{bmatrix} \dot{\mathbf{v}}_0 \\ \dot{\boldsymbol{\omega}} \end{bmatrix} = \begin{bmatrix} \mathbf{F}_I \\ \mathbf{M}_I \end{bmatrix} + \begin{bmatrix} \mathbf{F}_G \\ \mathbf{M}_G \end{bmatrix} + \begin{bmatrix} \mathbf{F}_{\mathrm{AS}} \\ \mathbf{M}_{\mathrm{AS}} \end{bmatrix} + \begin{bmatrix} \mathbf{F}_{\mathrm{AD}}(\mathbf{q}) \\ \mathbf{M}_{\mathrm{AD}}(\mathbf{q}) \end{bmatrix} + \begin{bmatrix} \mathbf{F}_C \\ \mathbf{M}_C \end{bmatrix} \tag{33}$$

where the inertial, gravity, and control terms are computed based on the rigid-body assumption [7], while the static deformation $\mathbf{q}$ is incorporated into the aerodynamic computation, that is, $\mathbf{F}_{\mathrm{AD}}$ and $\mathbf{M}_{\mathrm{AD}}$ are calculated by the method presented in Sec. III, with

$\dot{\mathbf{q}} = \ddot{\mathbf{q}} = \mathbf{0}$. This static deformation is solved from the following equation:

$$\mathbf{Kq} = u_0^2 \mathbf{M}_{ss}\mathbf{q} + u_0 \mathbf{M}_{sr}\boldsymbol{\upsilon} + \mathbf{Q}_V + \mathbf{Q}_F + \mathbf{Q}_{H(F)} + \mathbf{Q}_G + \mathbf{Q}_{\mathrm{AS}} \tag{34}$$

and it results from the generalized forces due to aerodynamics, aerostatics, and gravity. Specifically, the first two terms on the right-hand side are reduced from the potential-flow aerodynamics term in Eq. (20); the third to fifth terms are the generalized forces due to viscous effect, force on the fins, and force on the hull due to the fins, respectively, and they are obtained from Eqs. (23), (27), and (30) with $\dot{\mathbf{q}} = \mathbf{0}$; the last two terms are due to aerostatics and gravity and calculated from Eqs. (6) and (8), respectively.

The eigenvalue problem for this simplified dynamics model is solved to determine the longitudinal and lateral modes of the Skyship-500 and the corresponding eigenvalues are plotted, respectively, in Figs. 19 and 20. We observe that the third longitudinal rigid-body mode becomes unstable at approximately 82 m/s and the pitch/bending divergence occurs at 111 m/s, and that the instability speed for the first lateral rigid-body mode is 96 m/s. These results are approximately 10% lower than the corresponding speeds predicted by the full flexible model and, in this case, provide a conservative estimate. The computational time for the linearization and eigenvalue problem using the simplified dynamics model is approximately one-third of that using the full model.

Thus, under certain circumstances, this simplified model could be used to effectively provide meaningful results in predicting potential aeroelastic instabilities. One possible scenario might be to perform an initial analysis using the simplified model. This could be followed by the more complete analysis if the lowest predicted speed for instabilities falls in or close to the operating envelope of the airship. It should be noted, however, that the simplified model cannot be used to predict the flexible natural frequencies.

## VI. Conclusions

This paper proposes a theoretical framework for the dynamics modeling of flexible airships, which accounts for the interactions between the flight dynamics, structural dynamics, aerostatics, and aerodynamics. Specifically, the external forces, moments, and elastic generalized forces for the gravitational, aerostatic, aerodynamic, and control effects are developed in detail. To capture the coupling between the aerodynamic forces and structural elasticity, the local velocity distribution on the deformed vehicle is used in the computation of various aerodynamic forces. The elastic deformation is represented by time-dependent generalized coordinates and time-independent shape functions, the latter taken as natural vibration modes of an Euler–Bernoulli beam.

A dynamics simulation program was developed in the MATLAB environment and used to analyze the dynamics and frequency responses of the Skyship-500 airship. It was found that, generally speaking, the influence of flexibility on the airship motion is relatively small for the Skyship-500 in its operating speed range. The possibility of aeroelastic instability was investigated using two linearized dynamics models: the full flexible-body model and the quasi-static model. The aeroelastic instability of an airship is associated with the interaction between the aerodynamics, deformation, and rigid-body motion, because of the fact that the bending deflection reduces the aerodynamic effects that stabilize the airship against the Munk moment. As a result, some rigid-body modes can become unstable as the flight speed increases. The stability analysis of the Skyship-500 airship showed that the aeroelastic instability speeds of this airship are more than twice its operating speeds. Because the natural frequencies of elastic vibration

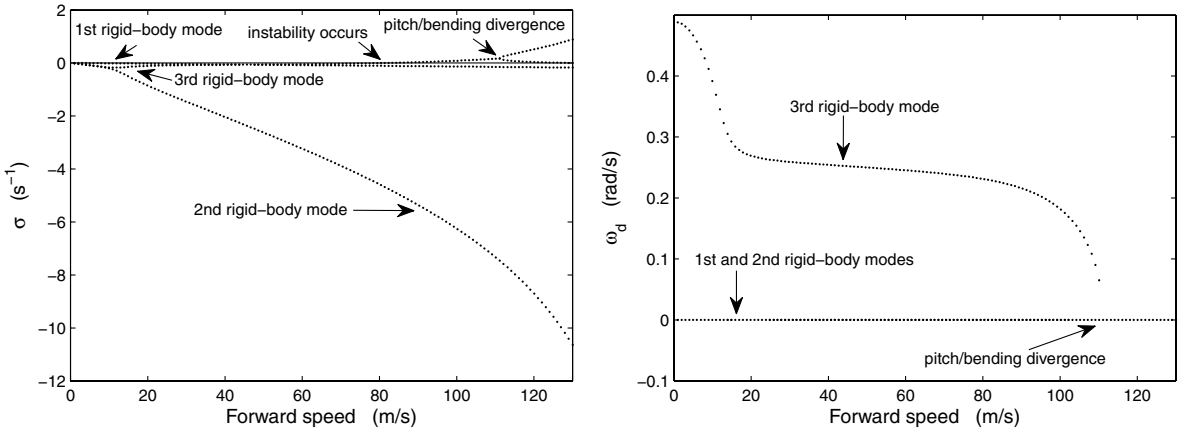


**Fig. 19 Eigenvalues of longitudinal modes from the simplified flexible model.**

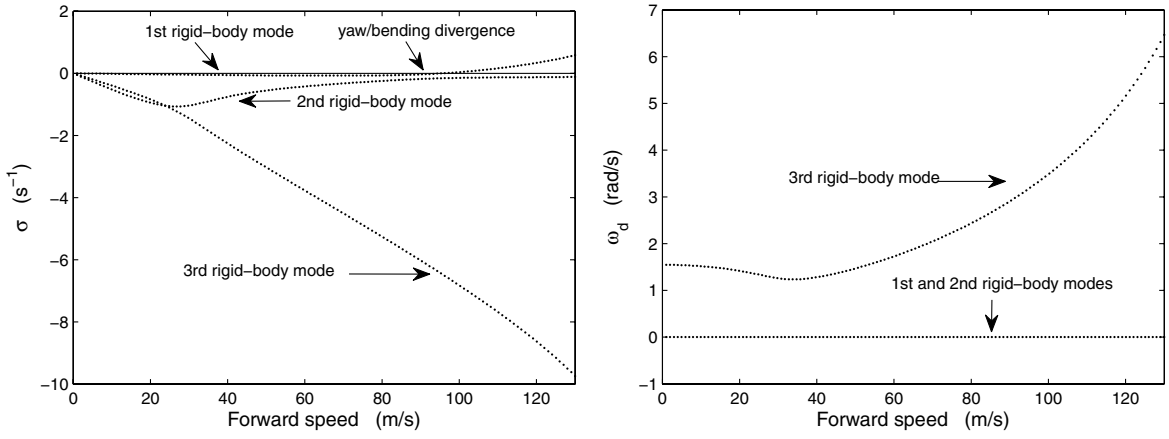


**Fig. 20 Eigenvalues of lateral modes from the simplified flexible model.**

are significantly higher than those of the rigid-body modes, the quasi-static model provides an effective and conservative tool for predicting the instability speeds of this airship.

The present dynamics simulation program provides results that demonstrate the interaction between the rigid-body motion, elastic deformation, and aerodynamic forces of an airship. It can be employed for other airship designs to evaluate their dynamics behavior and the possibility of aeroelastic instability. One important future research direction would be to develop methods to predict the onset of wrinkling and its impact on the dynamics of a flexible airship.

## References


[1] Khoury, G., and Gillett, J., *Airship Technology*, Cambridge Univ. Press, Cambridge, England, U.K., 1999, pp. 73–106, 141–209, 475–504.

[2] Tischler, M. B., Ringland, R. R., and Jex, H. R., "Heavy Airship Dynamics," *Journal of Aircraft*, Vol. 20, No. 5, 1983, pp. 425–433. doi:10.2514/3.44888

[3] Jex, H. R., and Gelhausen, P., "Pre- and Post-Flight-Test Models Versus Measured Skyship-500 Control Responses," *7th AIAA Lighter-Than-Air Technology Conference*, AIAA, New York, 1987, pp. 87–97.

[4] Amann, J. H., "A Comparison of a Nonlinear Flight Dynamic Simulation of an Airship with Flight Test Results," *7th AIAA Lighter-Than-Air Technology Conference*, AIAA, New York, 1987, pp. 78–86.

[5] Cook, M. V., Lipscombe, J. M., and Goineau, F., "Analysis of the Stability Modes of the Non-Rigid Airship," *The Aeronautical Journal*, Vol. 104, No. 1036, 2000, pp. 279–290.

[6] Schmidt, D. K., "Modeling and Near-Space Stationkeeping Control of a Large High-Altitude Airship," *Journal of Guidance, Control, and Dynamics*, Vol. 30, No. 2, 2007, pp. 540–547. doi:10.2514/1.24865

[7] Li, Y., and Nahon, M., "Modeling and Simulation of Airship Dynamics," *Journal of Guidance, Control, and Dynamics*, Vol. 30, No. 6, 2007, pp. 1691–1700. doi:10.2514/1.29061

[8] Evans, J. R., and DeLaurier, J. D., "The Shenandoah Flies Again: A Computer Simulation," *AIAA Lighter-Than-Air Systems Technology Conference*, AIAA, New York, 1981, pp. 62–73.

[9] Burgess, C. P., *Airship Design*, Ronald, New York, 1927, pp. 109–152.

[10] Hunt, J. D., "Structural Analysis of Aerostat Flexible Structure by the Finite Element Method," *Journal of Aircraft*, Vol. 19, No. 8, 1982, pp. 674–678. doi:10.2514/3.57448

[11] Amiryants, G. A., Grigorive, V. D., Ishmuratov, F. Z., Franz, A., d'Henin, E., and Kaempf, B., "Investigations of Airship Aeroelasticity," *23rd International Congress of Aeronautical Sciences*, International Congress of Aeronautical Sciences Paper ICAS-2002-4.6.1, 2002.

[12] Bessert, N., and Frederich, O., "Nonlinear Airship Aeroelasticity," *Journal of Fluids and Structures*, Vol. 21, No. 8, 2005, pp. 731–742. doi:10.1016/j.jfluidstructs.2005.09.005

[13] El Omari, K., Schall, E., Koobus, B., and Dervieux, A., "Inviscid Flow Calculation Around a Flexible Airship," *8th Conference of Applied Mathematics and Statistics*, Univ. of Zaragoza, Zaragoza, Spain, 2004, pp. 535–544.

[14] Bennaceur, S., Azouz, N., and Boukraa, D., "An Efficient Modelling of Flexible Airships," *8th Biennial ASME Conference on Engineering Systems Design and Analysis*, American Society of Mechanical Engineers, Fairfield, NJ, 2006, pp. 573–582.

[15] Schmidt, D. K., "Modeling and Simulation of Flexible Flight Vehicles," *Journal of Guidance, Control, and Dynamics*, Vol. 24, No. 3, 2001, pp. 539–546. doi:10.2514/2.4744

[16] Meirovitch, L., and Tuzcu, I., "Unified Theory for the Dynamics and Control of Maneuvering Flexible Aircraft," *AIAA Journal*, Vol. 42, No. 4, 2004, pp. 714–727. doi:10.2514/1.1489

[17] Platus, D. H., "Aeroelastic Stability of Slender, Spinning Missiles," *Journal of Guidance, Control, and Dynamics*, Vol. 15, No. 1, 1992, pp. 144–151. doi:10.2514/3.20812

[18] Patil, M. J., and Hodges, D. H., "Flight Dynamics of Highly Flexible Flying Wings," *Journal of Aircraft*, Vol. 43, No. 6, 2006, pp. 1790–1798. doi:10.2514/1.17640

[19] Cesnik, C., and Su, W., "Nonlinear Aeroelastic Modeling and Analysis of Fully Flexible Aircraft," *46th AIAA/ASME/ASCE/AHS/ASC Structures, Structural Dynamics and Materials Conference*, AIAA, Reston, VA, 2005.

[20] Main, J. A., Perterson, S. W., and Strauss, A. M., "Load-Deflection Behavior of Space-Based Inflatable Fabric Beams," *Journal of Aerospace Engineering*, Vol. 7, No. 2, 1994, pp. 225–238. doi:10.1061/(ASCE)0893-1321(1994)7:2(225)

[21] Suhey, J. D., Kim, N. H., and Niezrecki, C., "Numerical Modeling and Design of Inflatable Structures: Application to Open-Ocean-Aquaculture Cages," *Aquacultural Engineering*, Vol. 33, No. 4, 2005, pp. 285–303. doi:10.1016/j.aquaeng.2005.03.001

[22] McTavish, D. J., and Davidson, K., "Practical Large-Motion Modeling of Geometrically Complex Flexible Vehicles," *47th AIAA/ASME/ASCE/AHS/ASC Structures, Structural Dynamics, and Materials Conference*, AIAA, Reston, VA, May 1–4, 2006.

[23] Damaren, C., and Sharf, I., "Simulation of Flexible-Link Manipulators with Inertial and Geometric Nonlinearities," *Journal of Dynamic Systems, Measurement, and Control*, Vol. 117, No. 1, 1995, pp. 74–87. doi:10.1115/1.2798525

[24] Lamb, H., *Hydrodynamics*, 6th ed., Dover, New York, 1945, pp. 160–201.

[25] Macagno, E. O., and Landweber, L., "Irrotational Motion of the Liquid Surrounding a Vibrating Ellipsoid of Revolution," *Journal of Ship Research*, Vol. 2, No. 1, 1958, pp. 37–49.

[26] Munk, M. M., "The Aerodynamic Forces on Airship Hulls," NACA TR-184, 1924.

[27] Li, Y., "Dynamics Modeling and Simulation of Flexible Airships," Ph.D. Thesis, McGill Univ., Montreal, Jan. 2008.

[28] Freeman, H. B., "Pressure Distribution Measurements on the Hull and Fins of a 1/40-Scale Model of the U. S. Airship Akron," NACA TR-443, 1934.

[29] Belanger, P., *Control Engineering: A Modern Approach*, Saunders College Publishing, Orlando, FL, 1995, pp. 24–32.


E. Livne
*Associate Editor*